Article

Cell

Microbially Produced Imidazole Propionate Impairs Insulin Signaling through mTORC1

Graphical Abstract

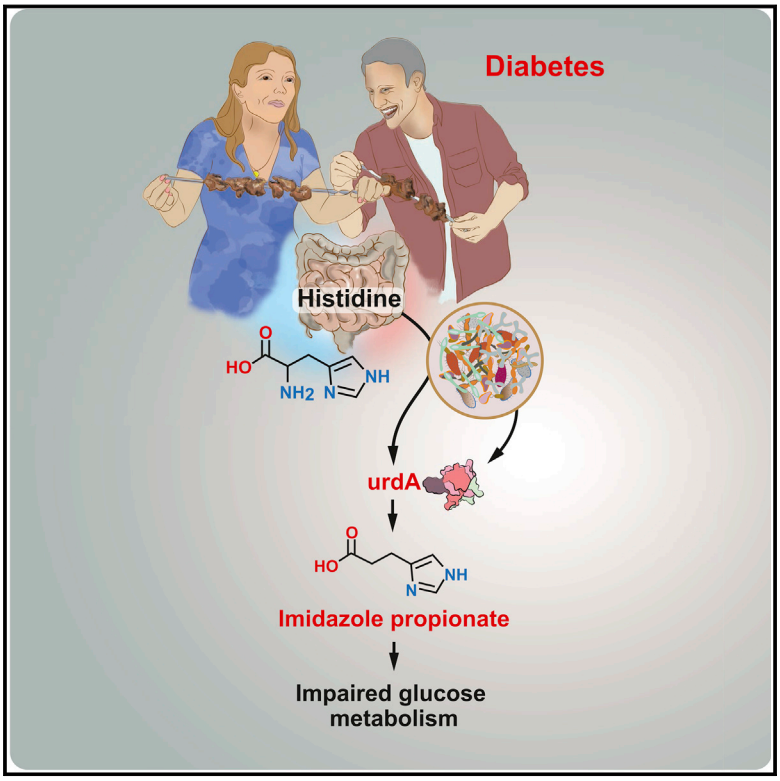

Authors

Ara Koh, Antonio Molinaro, Marcus Ståhlman, ..., Max Nieuwdorp, Göran Bergström, Fredrik Bäckhed

Correspondence

fredrik@wlab.gu.se

In Brief

Imidazole propionate, a metabolite produced by the gut microbiota, is elevated in type 2 diabetes and can directly impair glucose tolerance and insulin signaling.

Highlights

- Imidazole propionate levels are increased in subjects with type 2 diabetes (T2D)
- Imidazole propionate is produced from histidine by T2D-associated bacteria
- Imidazole propionate impairs glucose tolerance and insulin signaling
- Imidazole propionate inhibits IRS via activation of p38γ/p62/mTORC1

Koh et al., 2018, Cell *175*, 947–961
November 1, 2018 © 2018 Elsevier Inc.
https://doi.org/10.1016/j.cell.2018.09.055

CellPress

Cell

Microbially Produced Imidazole Propionate Impairs Insulin Signaling through mTORC1

Ara Koh,[1] Antonio Molinaro,[1] Marcus Ståhlman,[1] Muhammad Tanweer Khan,[1] Caroline Schmidt,[1,2] Louise Mannerås-Holm,[1] Hao Wu,[1] Alba Carreras,[1] Heeyoon Jeong,[3] Louise E. Olofsson,[1] Per-Olof Bergh,[1] Victor Gerdes,[4] Annick Hartstra,[5] Maurits de Brauw,[4] Rosie Perkins,[1] Max Nieuwdorp,[1,5,6] Göran Bergström,[1,2] and Fredrik Bäckhed[1,7,8,*]

[1]Department of Molecular and Clinical Medicine/Wallenberg Laboratory, Institute of Medicine, University of Gothenburg and Sahlgrenska University Hospital, Gothenburg, Sweden
[2]Department of Physiology, Sahlgrenska University Hospital, Gothenburg, Sweden
[3]Department of Life Sciences, Pohang University of Science and Technology, Pohang 37673, Republic of Korea
[4]Slotervaart Hospital, Amsterdam, the Netherlands
[5]Department of Vascular Medicine, Academic Medical Center, University of Amsterdam, Amsterdam, the Netherlands
[6]VU University Medical Center, Free University Amsterdam, Amsterdam, the Netherlands
[7]Novo Nordisk Foundation Center for Basic Metabolic Research, Section for Metabolic Receptology and Enteroendocrinology, Faculty of Health Sciences, University of Copenhagen, Copenhagen, Denmark
[8]Lead Contact
*Correspondence: fredrik@wlab.gu.se
https://doi.org/10.1016/j.cell.2018.09.055

SUMMARY

Interactions between the gut microbiota, diet, and the host potentially contribute to the development of metabolic diseases. Here, we identify imidazole propionate as a microbially produced histidine-derived metabolite that is present at higher concentrations in subjects with versus without type 2 diabetes. We show that imidazole propionate is produced from histidine in a gut simulator at higher concentrations when using fecal microbiota from subjects with versus without type 2 diabetes and that it impairs glucose tolerance when administered to mice. We further show that imidazole propionate impairs insulin signaling at the level of insulin receptor substrate through the activation of p38γ MAPK, which promotes p62 phosphorylation and, subsequently, activation of mechanistic target of rapamycin complex 1 (mTORC1). We also demonstrate increased activation of p62 and mTORC1 in liver from subjects with type 2 diabetes. Our findings indicate that the microbial metabolite imidazole propionate may contribute to the pathogenesis of type 2 diabetes.

INTRODUCTION

Metabolic disorders such as obesity, diabetes, and cardiovascular disease are associated with altered gut microbiota structure and function (Cotillard et al., 2013; Karlsson et al., 2013; Le Chatelier et al., 2013; Qin et al., 2012; Wang et al., 2011), and recent data suggest that the microbiota contributes to variations in metabolic responses to a given diet (Cotillard et al., 2013; Smith et al., 2013; Sonnenburg and Bäckhed, 2016). Studies assessing the effect of diet interventions on the microbiota have mostly focused on dietary fibers, which are precursors for bacterial fermentation, resulting in metabolites (short-chain fatty acids) that are associated with improved metabolism (Koh et al., 2016). However, recent studies have identified trimethylamine N-oxide (TMAO) as a microbiota-dependent metabolite that contributes to atherosclerosis in mouse models and associates with cardiovascular disease in humans (Koeth et al., 2013; Wang et al., 2011). In addition, branched-chain amino acids (BCAAs) (Pedersen et al., 2016; Ridaura et al., 2013; Shoaie et al., 2015), glutamate (Liu et al., 2017), and amino acid-derived uremic toxins (Aronov et al., 2011; Kikuchi et al., 2017) have been proposed as potentially harmful microbially modulated metabolites. Of note, a recent study identified a gut bacterial pathway that can metabolize aromatic amino acids into bioactive compounds (Dodd et al., 2017). However, there is little mechanistic insight into how amino acid-derived metabolites contribute to disease.

Here, we identify imidazole propionate as a microbially produced amino acid-derived metabolite that is present at higher concentrations in the portal and peripheral blood of subjects with type 2 diabetes. In addition, we identify bacteria that can produce imidazole propionate from urocanate. Furthermore, we show that imidazole propionate can worsen glucose tolerance when administered to mice and impairs insulin signaling at the level of insulin receptor substrate (IRS). Finally, we characterize the underlying signaling pathways.

RESULTS

Imidazole Propionate Is Associated with Type 2 Diabetes in Humans

Bacterial metabolites produced in the gut reach the liver through the portal vein and then enter the systemic circulation. To identify amino acid-derived microbial metabolites that may contribute to insulin resistance and type 2 diabetes, we first performed

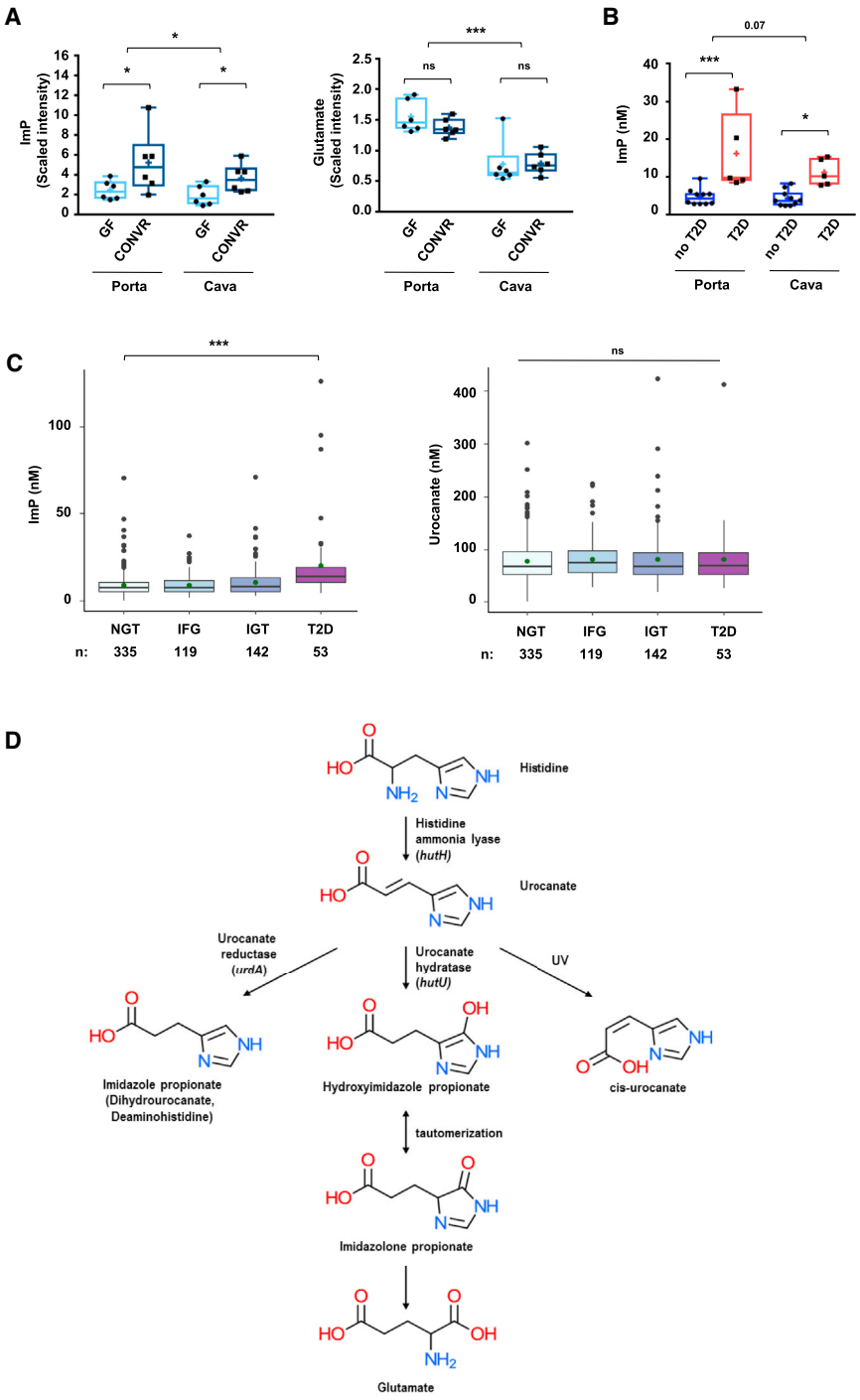

Figure 1. Imidazole Propionate Is Increased in Individuals with Type 2 Diabetes

(A) Relative levels of imidazole propionate (ImP) and glutamate in portal and vena cava plasma of GF and CONVR mice (n = 6 per group).

(B) Portal and peripheral plasma levels of ImP in obese BMI-matched subjects without type 2 diabetes (no T2D, n = 10) or with T2D (n = 5).

(C) Peripheral plasma levels of ImP or urocanate in humans with normal glucose tolerance (NGT), impaired fasting glucose (IFG), impaired glucose tolerance (IGT), and treatment-naive T2D.

(D) Histidine utilization pathway. Data presented as boxplots show minimum, 25% quartile, median, 75% quartile, maximum, and mean (marked as +). *p < 0.05, ***p < 0.001; ns, not significant. p values were determined by two-way ANOVA with repeated-measurements (A and B), Kruskal-Wallis test followed by Dunnett's test (C).

See also Figure S1 and Tables S1–S3.

untargeted metabolomics on plasma obtained from portal blood of 5 obese subjects (body mass index [BMI] > 40) with type 2 diabetes and 10 BMI-matched subjects without type 2 diabetes (Table S1). Only four amino acid-derived metabolites (dopamine sulfate, glutamate, imidazole propionate, and N-acetylputrescine) were significantly higher [false discovery rate (FDR) < 0.1] in the portal plasma of subjects with type 2 diabetes (Table S2). To focus on microbial metabolites only, we then investigated levels of these four metabolites in the global metabolomics profile of plasma from C57BL/6J germ-free (GF) and conventionally raised (CONVR) mice. We showed that imidazole propionate but not glutamate was present at higher levels both in the portal vein and vena cava plasma from the CONVR mice (Figure 1A); dopamine sulfate and N-acetylputrescine were not detected. We next developed a targeted method for imidazole propionate measurements and verified that the peak in the mice plasma has the same retention time and fragmentation pattern as those of a synthetic reference substance (Figure S1A). Using this analytical protocol, we also showed that antibiotic treatment of the CONVR mice reduced circulating imidazole propionate levels without significantly affecting body weight (Figures S1B and S1C), confirming the role of the microbiota in production of imidazole propionate. Targeted measurements of imidazole propionate in plasma obtained from portal and peripheral blood from the initial human cohort: (1) confirmed that concentrations of imidazole propionate were higher in the portal plasma of subjects with type 2 diabetes, and (2) showed that concentrations of imidazole propionate were also higher in the peripheral plasma of subjects with type 2 diabetes compared with those without type 2 diabetes (Figure 1B).

To validate our observation of increased concentrations of imidazole propionate in the peripheral blood of those with type 2 diabetes, we recruited 649 middle-aged individuals from the

Swedish population and divided them into four groups according to their level of glucose tolerance (Table S3). We observed significantly higher levels of imidazole propionate across the groups ($p < 0.0001$) and those with treatment-naive type 2 diabetes had higher levels of imidazole propionate compared with those with normal glucose tolerance after correcting for the potential confounding factors BMI, sex, and age ($p < 0.0001$) (Figure 1C). By contrast, the levels of its precursor, urocanate (Figure 1D), did not differ between the groups (Figure 1C).

To directly address if imidazole propionate is a microbially produced metabolite, we monitored the kinetics of imidazole propionate production in an *in vitro* gut simulator (a continuously fed stabilized microbial community maintained in an anaerobic, reducing environment mimicking that of the gut). After 1 week stabilization of the microbial communities from obese subjects with or without type 2 diabetes from the first cohort (n = 2 per group), we challenged the communities with 10 mM histidine and measured the levels of imidazole propionate for 7 hr. The bacterial communities from subjects without type 2 diabetes barely produced imidazole propionate at any time point whereas the bacterial communities from subjects with type 2 diabetes produced imidazole propionate after 1.5 hr and continued to produce imidazole propionate at the 7 hr time point (Figure 2A). To validate these findings, we performed batch culture and compared imidazole propionate production from histidine in bacterial communities from subjects with and without type 2 diabetes (n = 5 per group from the first cohort and n = 3 per group from the second cohort). End-point measurements showed that higher concentrations of imidazole propionate were produced in the presence of the type 2 diabetes-associated microbiota (Figures 2B and 2C). These observations suggest that type 2 diabetes-associated microbiota shunts urocanate to a lesser-known pathway to produce imidazole propionate (Figure 1D).

To identify bacteria that can produce imidazole propionate from urocanate, we performed large-scale screening for potential urocanate reductases (UrdAs) based on FAD-binding domains in the active sites (Figure S2A). We identified 812 UrdA homologs in bacterial genomes: 639 with conserved "H" and 173 without "H" (replaced with "Y" or "M") (Figure S2B; Table S4). We showed that bacteria with "Y"- or "M"-UrdA homologs but not those with "H"-UrdA homologs produced imidazole propionate from urocanate (Figure 2D); thus bacteria with "Y"- or "M"-UrdA homologs are authentic UrdA. Using a previously published metagenomics dataset that included subjects with treatment-naive type 2 diabetes and subjects with normal glucose tolerance (Karlsson et al., 2013), we identified 42 bacterial strains with authentic UrdA, 28 (67%) of which were more abundant in subjects with type 2 diabetes (Figure 2E). We noted, for example, that *Streptococcus mutans* and *Eggerthella lenta* (at the strain level), which we verified as imidazole propionate producers *in vitro* (Figure 2D), were more abundant in subjects with type 2 diabetes (Figure 2E), supporting an association between imidazole propionate production and the pathogenesis of type 2 diabetes.

Imidazole Propionate Impairs Glucose Tolerance and Insulin Signaling

To directly test whether imidazole propionate could affect glucose metabolism, we injected vehicle or imidazole propionate intraperitoneally into GF mice for 3 days. We observed that this treatment increased circulating concentrations of imidazole propionate from 1.4 nM to around 13 nM without affecting urocanate concentrations (Figure 3A) and increased imidazole propionate levels in the liver (Figure S3A). The presence of low concentrations of imidazole propionate in vehicle-injected GF mice is likely explained by the fact that the chow diet fed to the mice contained imidazole propionate (Figure S3B). Importantly, glucose intolerance was induced in imidazole propionate-injected GF mice (Figure 3B), supporting a role for imidazole propionate as a plausible contributor to impaired glucose metabolism *in vivo*. However, insulin levels were not affected by imidazole propionate (Figure S3C). We also observed that hepatic expression of *G6pase* and *Pepck*, genes for key rate-limiting gluconeogenic enzymes, was significantly increased in imidazole propionate-injected GF mice compared with controls (Figure 3C). However, imidazole propionate did not affect hepatic expression of *Srebp1c* and *Fasn*, key lipogenic genes (Figure 3C).

We also showed that 3-day injections of imidazole propionate in CONVR mice increased concentrations of imidazole propionate in the circulation and in the liver (Figures 3D and S3D). Of note, imidazole propionate treatment impaired glucose tolerance (Figure 3E) without any significant effect on body weight, liver and white adipose tissue (WAT) weight, food intake, or insulin levels (Figures S3E–S3H). Energy expenditure in the early dark phase was significantly reduced by imidazole propionate; however, total locomotor activity was not significantly reduced by imidazole propionate treatment (Figures S3I–S3K). By implanting slow-releasing pellets containing either placebo or imidazole propionate in CONVR mice, we showed that long-term treatment (14 days) with imidazole propionate caused significant impairment of glucose tolerance (Figure 3F) without affecting body weight, liver and WAT weight, or insulin levels (Figures S3L–S3O).

We next investigated the effect of imidazole propionate injections on key proteins involved in insulin signaling in mice. We found that 3-day injections of imidazole propionate in GF mice did not affect hepatic levels of the insulin receptor (IR) or basal Akt phosphorylation (S473) but reduced hepatic levels of IRS1 and IRS2 (Figure 3G). These reductions occurred post-transcriptionally because there were no significant changes in hepatic *Irs1* and *Irs2* mRNA levels (Figure S3P). We also showed a reduction of IRS2 (but not IRS1) in muscle (Figure 3H) and of IRS1 (but not IRS2) in WAT (Figure 3I). Imidazole propionate treatment for 3 days did not affect IRS protein levels in CONVR mice (Figure S3Q). However, 14-day treatment with imidazole propionate reduced IRS2 levels in liver and muscle of CONVR mice without reducing IRS1 levels; a trend toward a reduction in IRS1 was observed in WAT, but IRS2 was not detected (Figure S3R). Previous reports have shown that insulin has different effects on IRS1 or IRS2 reduction depending on the cell type and even on the differentiation status of the same cell type (Rui et al., 2001).

To further investigate the role of imidazole propionate on insulin signaling, we used primary hepatocytes. Incubation with imidazole propionate for 8 hr did not affect IRS1 levels but significantly blunted insulin-induced IRS1 Y612 phosphorylation (Figure 3J), which is required for insulin-stimulated activation of IRS1-associated phosphatidylinositol-3 kinase and downstream

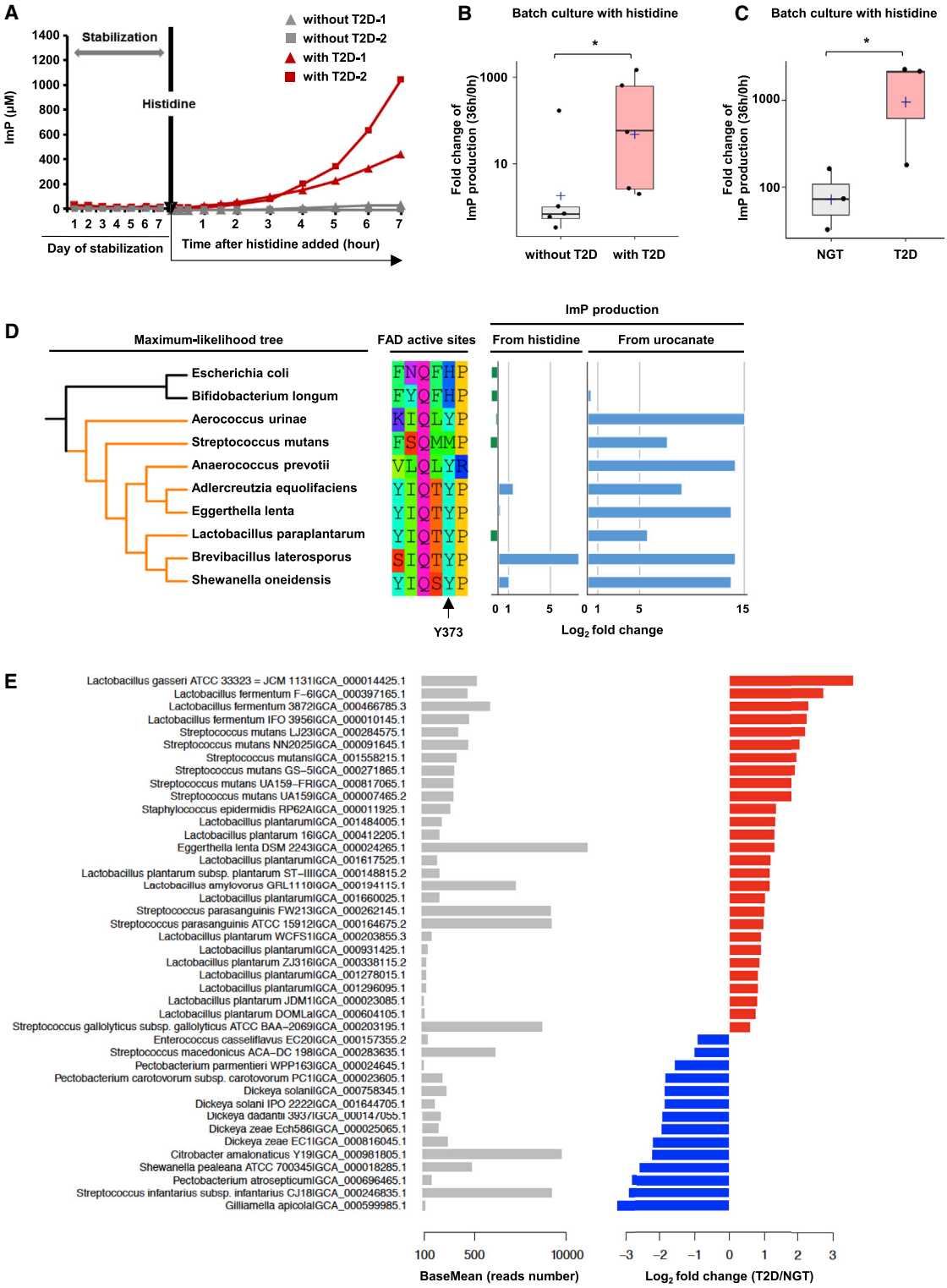

Figure 2. Imidazole Propionate Is Microbially Produced

(A) Production of imidazole propionate (ImP) from 10 mM histidine in an *in vitro* gut simulator inoculated (in separate experiments) with feces from two subjects without type 2 diabetes (T2D) or from two subjects with T2D.

(B) End-point measurements of ImP production from 10 mM histidine in batch culture experiments using feces from obese BMI-matched subjects without T2D (n = 5) or with T2D (n = 5).

(legend continued on next page)

Akt (Esposito et al., 2001). In addition, we showed that 20 hr incubation of hepatocytes with imidazole propionate reduced IRS1 and IRS2 levels (Figure 3K) and significantly inhibited insulin-stimulated Akt phosphorylation (Figure 3L).

We also noted that IRS1 levels were reduced by 8 hr treatment of imidazole propionate in the human embryonic kidney cell line HEK293 (Figure 3M), indicating that imidazole propionate acts through a pathway that is conserved across cell types (although its effect was more rapidly induced in HEK293 cells than in primary hepatocytes). In addition, we showed that the imidazole propionate-induced reduction in IRS levels in HEK293 cells was inhibited by the proteasome inhibitor MG132 (Figure 3M), suggesting the involvement of a proteasome-dependent pathway.

Together, these data show that imidazole propionate has negative impacts on insulin signaling at the level of IRS (i.e., inhibiting tyrosine phosphorylation or reducing protein levels).

Imidazole Propionate Activates mTORC1

We speculated that imidazole propionate inhibits insulin signaling through mTORC1, which is known to induce IRS serine phosphorylation leading to inhibition of IRS tyrosine phosphorylation and/or proteasomal degradation of IRS (Harrington et al., 2004; Leontieva et al., 2014; Ozes et al., 2001). In agreement with our hypothesis, we showed that: (1) imidazole propionate as well as leucine, a well-known mTORC1 activator, increased phosphorylation of S6K1 (a marker of mTORC1 activation) in primary hepatocytes; and (2) rapamycin and torin 1 (inhibitors of mTORC1 and mTORC1/2, respectively) inhibited the imidazole propionate-induced increase in S6K1 phosphorylation and reduction in IRS levels (Figures 4A, S4A, and S4B).

In HEK293 cells, mTORC1 depletion by Raptor knockdown prevented imidazole propionate-mediated induction of IRS1 S636/S639 phosphorylation and inhibition of insulin-stimulated IRS1 tyrosine phosphorylation; however, this treatment did not completely reverse imidazole propionate-induced S6K1 phosphorylation or prevent imidazole propionate-induced IRS1 reduction, possibly due to incomplete knockdown of Raptor (Figure 4B).

mTORC1 can only induce S636/S639 phosphorylation of IRS1 *in vitro*; however, S6K1 induces serine phosphorylation on multiple sites of IRS1 *in vivo*, which is required for IRS1 degradation (Harrington et al., 2004; Leontieva et al., 2014; Ozes et al., 2001; Shah and Hunter, 2006; Tzatsos, 2009). We showed that S6K1 knockdown in HEK293 cells inhibited imidazole propionate-induced induction of IRS1 S636/S639 phosphorylation, inhibition of insulin-stimulated IRS1 tyrosine phosphorylation, and reduction of IRS1 levels (Figure 4B). Because IRS serine phosphorylation is known to precede IRS degradation (Harrington et al., 2004; Leontieva et al., 2014; Ozes et al., 2001), we suggest that imidazole propionate can have impacts on both IRS1 serine phosphorylation and subsequent degradation. Furthermore, S6K1 knockdown promoted hypersensitivity to insulin as observed by higher insulin-induced phosphorylation of Akt in the presence of imidazole propionate, which likely caused activation of the S6K1 remaining after incomplete knockdown (Figure 4B).

Consistent with our hypothesis that imidazole propionate signals through mTORC1, we observed that 3-day imidazole propionate treatment *in vivo* increased S6K1 phosphorylation in the liver, soleus muscle, and WAT of CONVR mice (Figure 4C). This treatment also increased S6K1 phosphorylation in the liver of GF mice without affecting mTOR S2481 autophosphorylation or autophagy (Figure 4D). In addition, we showed that imidazole propionate promoted a time-dependent increase in S6K1 phosphorylation in HEK293 cells (Figure 4E).

In contrast to insulin, which induces mTOR S2481 autophosphorylation but cannot activate mTORC1 in the absence of amino acids (Soliman et al., 2010; Wang et al., 2005), imidazole propionate did not promote mTOR S2481 autophosphorylation in HEK293 cells (Figure 4E) but induced S6K1 phosphorylation in amino acid-deprived primary hepatocytes (Figure 4F). We also showed that 1 hr incubation with imidazole propionate in amino acid-deprived HEK293 cells induced S6K1 phosphorylation to a similar extent as that induced by amino acid stimulation for 1 hr (Figure S4C). Moreover, in amino acid-deprived HEK293 cells, imidazole propionate induced phosphorylation of S2448 but not S2481 of mTORC1 (Figure 4G). This is consistent with previous results showing that mTORC1 activity associates with phosphorylation of S2448 but not S2481 of mTORC1 (Copp et al., 2009).

Earlier studies have shown that amino acid-induced mTORC1 activation requires mTORC1 localization to the lysosome, which is mediated by the formation of a complex between the active Rag heterodimer RagA/B-GTP/RagC/D-GDP and mTORC1 (Raptor and mTOR) (Duran et al., 2011; Sancak et al., 2008). We showed that imidazole propionate also induced lysosomal localization of mTOR in amino acid-deprived HEK293 cells (Figure 4H) and that RagA/B-GDP and RagC/D-GTP, which are inactive Rag GTPases, blocked the imidazole propionate-induced S6K1 phosphorylation (Figure S4D). Moreover, the active Rag GTPases RagA/B-GTP did not further increase S6K1 phosphorylation (Figure S4D). By performing immunoprecipitation with FLAG-tagged mTOR and monitoring interaction with HA-tagged Raptor and Myc-tagged Rag GTPases, we showed that imidazole propionate induced formation of the mTORC1-Rag heterodimer (Figure S4E). In addition, we observed that imidazole

(C) End-point measurements of ImP production from 10 mM histidine in batch culture experiments using feces from subjects with normal glucose tolerance (NGT) (n = 3) or with treatment-naive T2D (n = 3).

(D) Prediction of ImP-producing bacteria and experimental validation using histidine or urocanate as substrate. ImP production shown as log transformed fold-change compared with blank samples.

(E) Abundance of bacteria with "non-H"-UrdA in subjects with treatment-naive T2D (n = 33) or with NGT (n = 43) from a previously published metagenomic dataset (Karlsson et al., 2013). Bacterial strains that were significantly higher or lower in subjects with T2D compared with subjects with NGT are shown as red or blue bars, respectively (cut-off 100 reads; FDR < 0.05).

Data presented as boxplots show minimum, 25% quartile, median, 75% quartile, maximum, and mean (marked as +). *p < 0.05. p values were determined by Wilcoxon one-tailed test (B and C).

See also Figure S2 and Table S4.

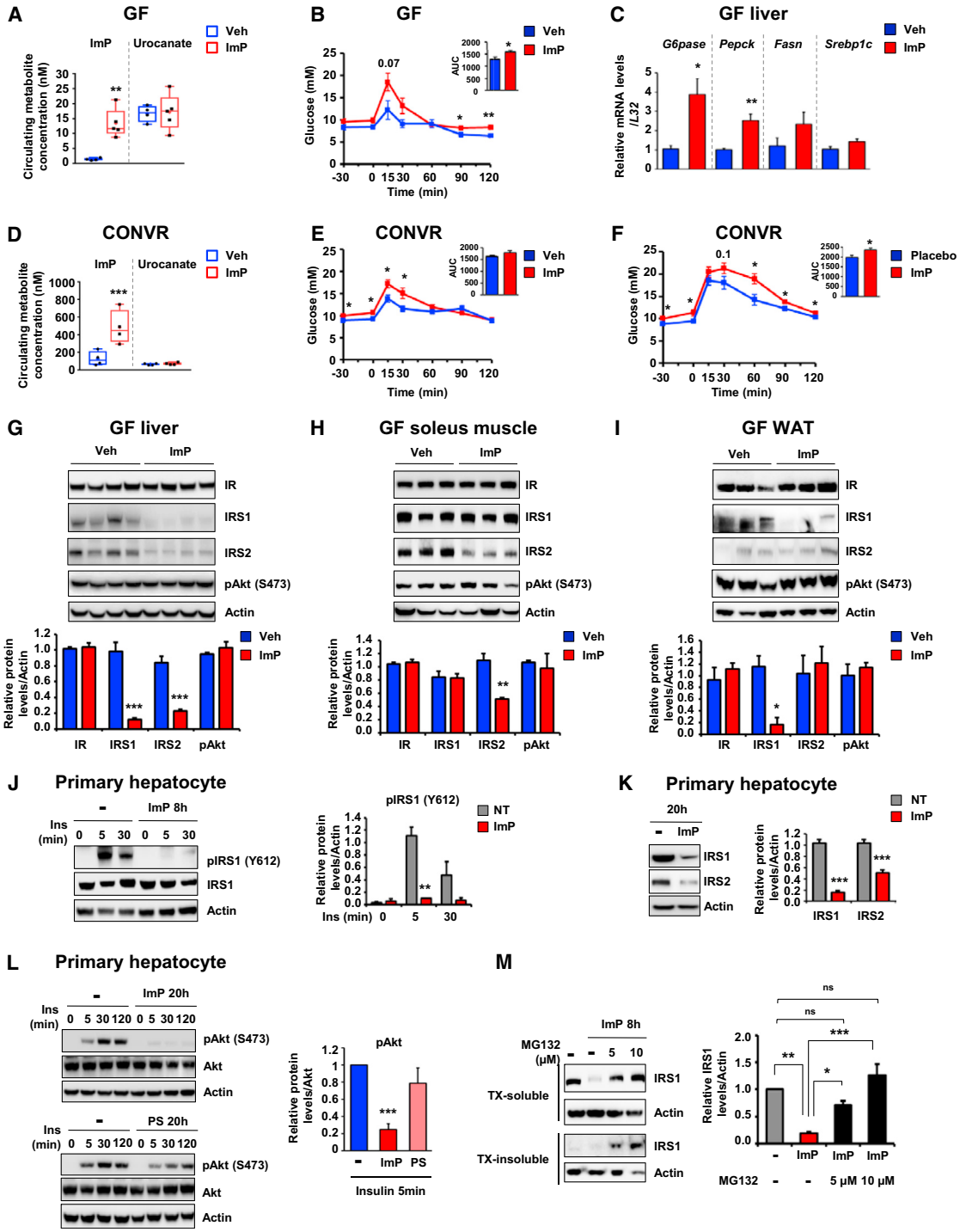

Figure 3. Imidazole Propionate Impairs Glucose Tolerance and Insulin Signaling

(A–C) Plasma levels of imidazole propionate (ImP) and urocanate (A), intraperitoneal glucose tolerance test (B), and expression of genes involved in gluconeogenesis and lipogenesis in GF mice after intraperitoneal injection of vehicle (C) (Veh, 1% DMSO in water; n = 4) or ImP (500 μg; n = 5) twice per day for 3 days.

(D) Plasma levels of ImP and urocanate in CONVR mice after intraperitoneal injection of vehicle (n = 4) or ImP (100 μg; n = 4) twice per day for 3 days.

(E) Intraperitoneal glucose tolerance test in CONVR mice injected with vehicle (n = 6) or ImP (100 μg; n = 5).

(F) Intraperitoneal glucose tolerance test in CONVR mice implanted with pellets containing placebo (n = 5) or ImP (n = 6) for 14 days (350 μg/day).

(G–I) Immunoblot (and quantification) of (G) liver lysates, (H) soleus muscle lysates, and (I) white adipose tissue (WAT) lysates from GF mice showing effect of 3-day treatment with vehicle or ImP (500 μg twice per day) on insulin signaling components.

(J) Effect of ImP (100 μM for 8 hr) on insulin (Ins)-stimulated IRS1 tyrosine phosphorylation in primary hepatocytes (n = 3).

(legend continued on next page)

propionate could promote mTORC1/RagB complex formation in the presence of amino acids (Figure S4F), indicating that imidazole propionate can act as an mTORC1 activator in (patho) physiological conditions *in vivo* (i.e., in the presence of amino acids).

Imidazole Propionate-Induced mTORC1 Activation Is Dependent on p62 Phosphorylation

Phosphorylation of the adaptor protein p62 at T269 and S272 has recently been shown to be critical for amino acid induction of mTORC1 activation (Linares et al., 2015). Here, we showed that imidazole propionate induced p62 phosphorylation in liver and primary hepatocytes from CONVR mice (Figures 5A and 5B). In primary hepatocytes, this response was not affected by rapamycin or torin 1 (Figure 5B), indicating that mTORC1 is downstream of p62 phosphorylation. Imidazole propionate promoted a concentration-dependent increase in p62 phosphorylation in HEK293 cells, with activation observed at concentrations as low as 10 nM in the absence of amino acids (Figure S5A). Compared with p62, S6K1 and IRS1 S636/S639 were less sensitive to imidazole propionate (Figure S5A), again supporting a role for p62 phosphorylation upstream of mTORC1. Furthermore, p62 knockdown by small interfering RNA (siRNA) reduced imidazole propionate-induced S6K1 and IRS1 S636/S639 phosphorylation (Figure 5C). Together these data suggest that p62 is a mediator of imidazole propionate-induced mTORC1 activation. Of note, neither p62 nor S6K1 was phosphorylated by histidine, its metabolites urocanate and glutamate, or the structurally similar bacterial metabolite indole propionate (Figure 5D), highlighting the specificity of imidazole propionate.

We next determined if the p62 phosphorylation-deficient mutant T269A/S272A could block imidazole propionate-induced signaling in HEK293 cells. We first showed that this protein is a dominant-negative mutant as it reduced imidazole propionate-induced p62 phosphorylation (Figures 5E and 5F). Both in the absence and presence of amino acids, expression of p62 T269A/S272A: (1) inhibited imidazole propionate-induced phosphorylation of S6K1 and IRS1 (S636/S639) (Figures 5E and 5F); and (2) disrupted imidazole propionate-induced complex formation between mTORC1 and RagB (Figures S5B and S5C). Although the detailed mechanism of action needs to be investigated further, these data indicate that p62 phosphorylation at T269/S272 promotes transmission of the imidazole propionate signal to mTORC1.

Alternative p38 Promotes Imidazole Propionate-Induced p62 and mTORC1 Activation

There are four p38 mitogen-activated protein kinase (MAPK) isoforms in mammalian cells, which can be divided into two subsets depending on their substrate specificity: p38α/p38β and p38γ/p38δ (also called alternative p38 MAPK) (Cuenda and Rousseau, 2007). A recent study reported that p38δ, but not p38α/p38β nor p38γ, is required to mediate the amino acid-induced activation of p62 and mTORC1 in HEK293 cells (Linares et al., 2015). Here, we showed that knockdown of p38α or p38β in HEK293 cells did not affect p62 and mTORC1 activation (Figure 6A). Although knockdown of p38δ partly inhibited imidazole propionate-induced phosphorylation of p62 and S6K1, it did not affect IRS1 (Figures 6B and S6A). By contrast, p38γ knockdown blocked imidazole propionate-induced phosphorylation of p62, S6K1, and IRS1 S636/S639 in amino acid-deprived HEK293 cells (Figures 6B and S6B). Furthermore, we showed that p38γ but not p38δ was expressed in primary hepatocytes whereas HEK293 cells express both isoforms (Figure S6C); despite this difference, imidazole propionate had similar effects on p62 phosphorylation in both cell types (Figures 5B and 5D). Thus, although we cannot exclude a role for p38δ in imidazole propionate-induced mTORC1 signaling in some cell types, our data show that p38γ potentially plays a greater role in mediating the signal from imidazole propionate to activation of p62 and mTORC1. Of note, we also showed that p38γ knockdown inhibited IRS reduction induced by 8 hr incubation with imidazole propionate in HEK293 cells in the presence of amino acids (Figure 6C).

By performing an *in vitro* kinase assay, we showed that p62 phosphorylation (at T269 and S272) was induced by p38γ in the presence of 50 μM ATP, which was further increased with 200 μM ATP (Figure 6D), identifying p38γ as a direct kinase for p62 phosphorylation. Importantly, imidazole propionate enhanced p62 phosphorylation in a concentration-dependent manner (Figure 6D), indicating that imidazole propionate could directly promote p38γ activity *in vitro*. The activation of p38 MAPKs including p38γ is known to be mediated by phosphorylation at T180/Y182 by upstream kinases. ATP itself did not induce p38γ autophosphorylation; however, imidazole propionate together with ATP induced p38γ autophosphorylation. Although upstream kinase-mediated p38 phosphorylation is the conventional mechanism to activate p38, there are studies that support p38 autophosphorylation and thus suggest that p38 can activate itself (Ashwell, 2006; Beenstock et al., 2014; Ge et al., 2002; Kim et al., 2005).

Imidazole Propionate Associates with p62 and S6K1 Phosphorylation in Human Liver

Consistent with our initial observation that imidazole propionate concentrations were higher in individuals with versus those without type 2 diabetes (Figure 1B), we showed that phosphorylation of p62 and S6K1 was higher in liver from subjects with

(K) Effect of long-term ImP treatment (100 μM for 20 hr) on IRS protein levels in primary hepatocytes (n = 7).
(L) Effect of ImP or the tyrosine-derived microbial metabolite phenol sulfate (PS) (both 100 μM for 20 hr) on Akt activation simulated by insulin (5 nM) in primary hepatocytes (n = 4).
(M) Effect of the proteasome inhibitor MG132 on IRS reduction induced by ImP (100 μM) in serum-starved HEK293 cells (n = 3); cells were co-treated with MG132 and ImP for 8 hr. TX, triton.
Data in (A) and (D) are presented as boxplots and show minimum, 25% quartile, median, 75% quartile, and maximum. Other data are shown as mean ± SEM. *$p < 0.05$, **$p < 0.01$, ***$p < 0.001$. Two-way ANOVA with repeated-measurements followed by Sidak multiple comparisons test (A and D) and unpaired two-tailed Student's t tests (B–L). One-way ANOVA followed by Tukey's multiple comparisons test (M).
See also Figure S3.

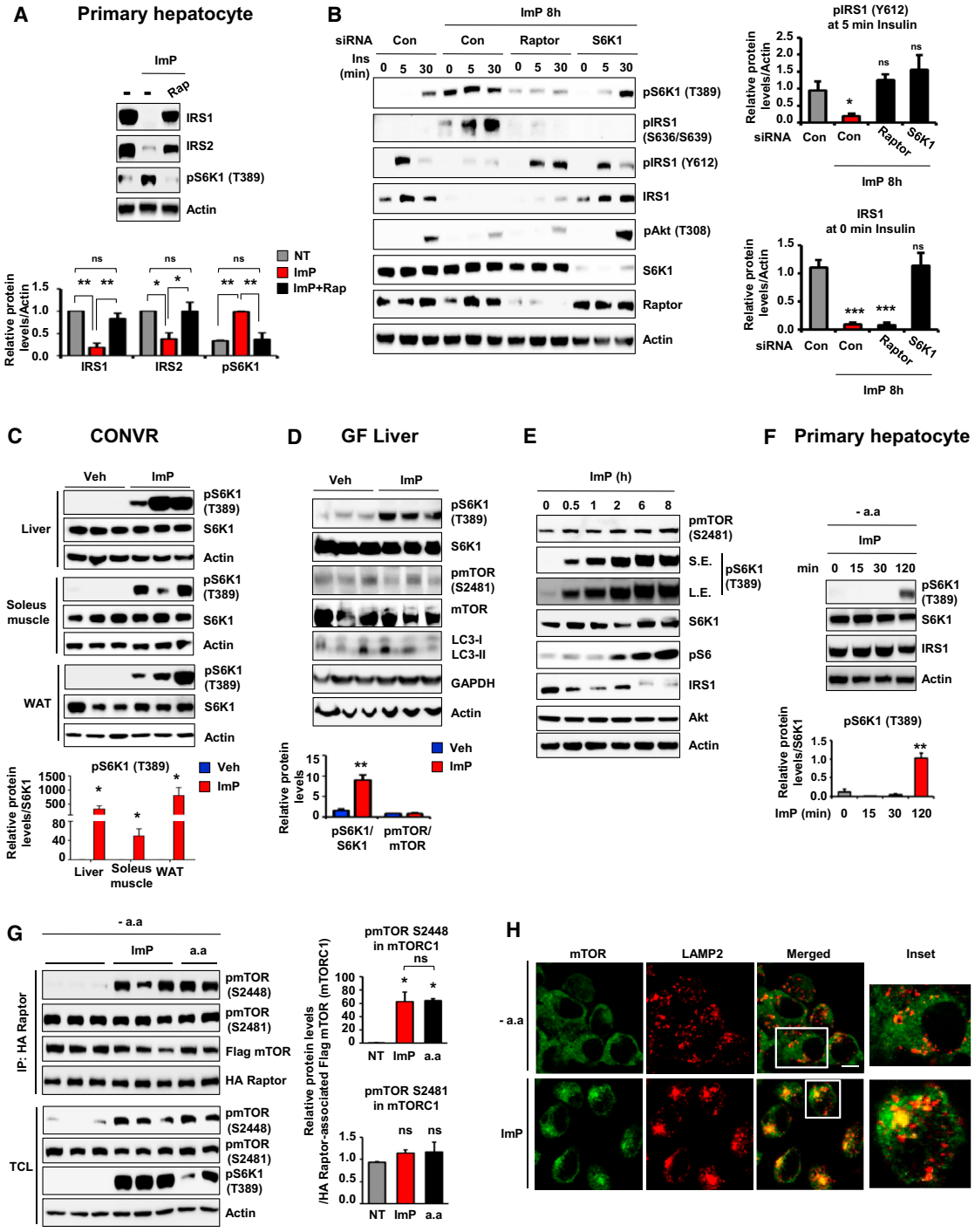

Figure 4. Imidazole Propionate Activates mTORC1

(A) Rapamycin (Rap, 20 nM) inhibits the effect of imidazole propionate (ImP) (100 μM for 20 hr) on IRS and pS6K1 in primary hepatocytes (n = 3).

(B) Immunoblot showing involvement of mTORC1-dependent pathway in ImP-induced impairment of insulin signaling. HEK293 cells were transfected with control siRNA (Con), Raptor siRNA, or S6K1 siRNA, serum starved for 18 hr, pretreated with ImP (100 μM for 8 hr), and then stimulated with 5 nM insulin (n = 4).

(C) Immunoblot of liver, soleus muscle, and WAT lysates from CONVR mice showing that 3-day treatment with vehicle (Veh) or ImP (100 μg twice per day) increases phosphorylation of S6K1 (n = 3).

(D) Immunoblot of liver lysates from GF mice showing that 3-day treatment with vehicle or ImP (500 μg twice per day) increases phosphorylation of S6K1 but not mTOR S2481 (n = 3).

(E) Immunoblot of serum-starved HEK293 cells incubated with 100 μM ImP for the time indicated (n = 2). S.E., short exposure, L.E., long exposure.

(legend continued on next page)

type 2 diabetes than in those without type 2 diabetes (n = 5 and 7, respectively, from the initial cohort) (Figure 7A). We did not observe any difference in hepatic IRS1 levels between those with and without type 2 diabetes, but IRS2 levels were significantly lower in subjects with type 2 diabetes (Figure 7A). Although mTORC1 activation is known to promote the degradation of both IRS1 and IRS2, either IRS1 or IRS2 can be targeted for proteasomal degradation depending on the cell type (Rui et al., 2001). We did not observe any differences in mTOR S2481 phosphorylation (i.e., autophosphorylation) or in phosphorylation of AMPK T172 and Akt S473, two known upstream regulators of mTORC1 (Yang and Guan, 2007) (Figure 7A). Furthermore, correlation analysis showed that: (1) plasma HbA1c positively associated with phosphorylation of p62 and S6K1 but not with phosphorylation of AMPK and Akt; (2) plasma HbA1c negatively associated with IRS2 in the liver; (3) there was a positive correlation between p62 and S6K1 phosphorylation; and (4) portal levels of imidazole propionate positively correlated with p62 and S6K1 phosphorylation (Figures 7B and 7C). These data are consistent with a role for imidazole propionate in impairing insulin signaling through the p62 and mTORC1 pathway.

Previous studies have shown that BCAAs are associated with insulin resistance (Pedersen et al., 2016) and that they activate p62 and mTORC1 (Linares et al., 2015). However, although we showed that portal levels of imidazole propionate from these subjects positively correlated with phosphorylation of p62 and S6K1, we did not observe any significant correlations between BCAAs and phosphorylation of p62 and S6K1 (Figure 7C).

DISCUSSION

We have identified imidazole propionate as a microbially produced histidine-derived metabolite that is increased in subjects with type 2 diabetes. We also identified bacteria that could produce imidazole propionate and showed that imidazole propionate treatment impairs glucose tolerance in mice. We further showed that imidazole propionate inhibits insulin signaling at the level of IRS through activation of the p38γ/p62/mTORC1 pathway at the cellular level (Figure 7D). Finally, consistent with a potential role for imidazole propionate in impairment of insulin signaling in humans, we showed increased activation of p62 and mTORC1 in liver from subjects with type 2 diabetes.

An earlier study reported that imidazole propionate is excreted from patients with intestinal disorders but is almost absent in feces and urine from healthy subjects (van der Heiden et al., 1972), supporting the concept of imidazole propionate as a microbial metabolite with detrimental health effects. Our results showing that imidazole propionate is not only present at higher concentrations in subjects with type 2 diabetes but is present at similar concentrations in the portal and peripheral blood indicate that this metabolite could have systemic effects.

To modify the production of microbial metabolites, it is important to identify the metabolic pathways required for their production. Histidine degradation pathways leading to the production of urocanate and glutamate are well conserved both in bacteria and humans (Bender, 2012). However, the bacterial UrdA, which catalyzes the production of imidazole propionate from urocanate, has only recently been discovered (in *Shewanella oneidensis*) (Bogachev et al., 2012). A major hurdle to identifying UrdAs is their high sequence homology with fumarate reductase and succinate dehydrogenase. Here, we showed that bacteria with "Y" or "M"-UrdA homologs (without "H") are authentic UrdAs and further showed increased abundance of strains with the capability of producing imidazole propionate in subjects with type 2 diabetes. We speculate that a shift in the gut environment resulting from dietary changes and/or an altered immune system (Schroeder and Bäckhed, 2016) can contribute to the expansion of imidazole propionate-producing bacteria. Because urocanate can be used as an electron acceptor in UrdA-containing bacteria, depletion of other common electron acceptors such as fumarate, ferric ion, and nitrate may confer a growth benefit to these bacteria (Bogachev et al., 2012). In addition, because UrdA is active at neutral pH (Bogachev et al., 2012) and the proximal colon has an acidic pH, increases in pH, possibly resulting from decreased production of short-chain fatty acids and increased protein fermentation in the gut (Windey et al., 2012), may increase production of imidazole propionate. Accordingly, clarification of the interplay between diets, bacteria, and the gut environment would be important to understand how to modify imidazole propionate production in humans.

In this study, we demonstrated the signaling potential of imidazole propionate by identifying alternative p38 MAPK as a target of imidazole propionate. Alternative p38 MAPK has a broad spectrum of tissue expression (Beardmore et al., 2005), and both p38γ and p38δ are implicated in pathological conditions including impaired glucose tolerance (González-Terán et al., 2016). Moreover, because imidazole propionate induced sustained activation of mTORC1, it is thus potentially linked to pathological conditions related to mTORC1 hyperactivation not only in diabetic complications (retinopathy, nephropathy, and heart failure) but also in cancer (Blagosklonny, 2013).

Although BCAAs have been suggested to link hyperactivation of mTORC1 with insulin resistance, several studies have demonstrated that dietary supplementation with BCAAs improves metabolic health (Chen and Reimer, 2009; Layman and Walker, 2006; Mojtahedi et al., 2011; Muto et al., 2006; Qin et al., 2011;

(F) Rapid effects of ImP (100 μM) on pS6K1 in amino acid-deprived primary hepatocytes (n = 3).

(G) Effects of ImP or amino acids (a.a) on mTORC1-associated mTOR phosphorylation. HEK293 cells transfected with Flag mTOR and HA Raptor were serum- and amino acid-deprived, stimulated with ImP or a.a for 2 hr and subjected to mTORC1 immunoprecipitation with HA Raptor (n = 3 for control and ImP and n = 2 for a.a).

(H) Images of amino acid-deprived HEK293 cells incubated with ImP (100 μM for 1 hr) and co-immunostained for mTOR and LAMP2, showing lysosomal localization of mTOR. Scale bar, 10 μm.

Data are mean ± SEM. *$p < 0.05$, **$p < 0.01$, ***$p < 0.001$; ns, not significant. One-way ANOVA followed by Tukey's test (A and G), one-way ANOVA followed by Dunnett's test (B), and unpaired two-tailed Student's t tests (C, D, and F).

See also Figure S4.

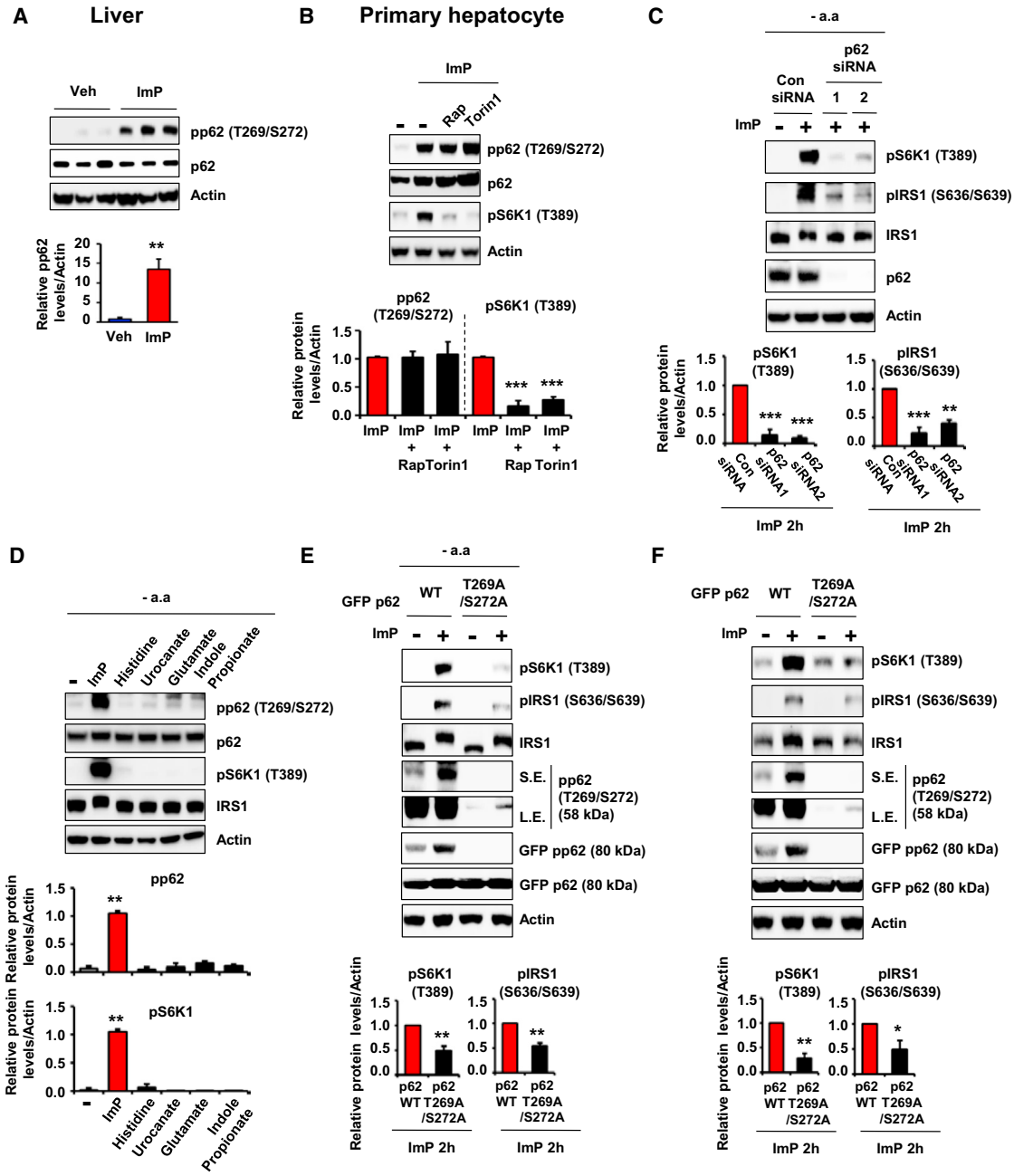

Figure 5. Imidazole Propionate Induces p62 Phosphorylation Upstream of mTORC1

(A) Immunoblot of liver lysates from CONVR mice showing that 3-day treatment with vehicle (Veh) or imidazole propionate (ImP) (100 μg twice per day) increases phosphorylation of p62 (n = 3).

(B) Effect of ImP (100 μM), rapamycin (Rap, 20 nM), or Torin1 (250 nM) for 12 hr on p62 phosphorylation (T269 and S272) in primary hepatocytes (n = 3).

(C) Effect of p62 knockdown on ImP-induced signaling. HEK293 cells were transfected with control siRNA (Con siRNA) or non-overlapping siRNAs against p62 (p62 siRNA1 or siRNA2) and incubated with ImP (100 μM) in the absence of amino acids (−a.a) for 2 hr (n = 3).

(D) Effect of ImP, histidine, urocanate, glutamate, or indole propionate (100 μM for 1 hr) on p62 phosphorylation in amino acid-deprived HEK293 cells (n = 2).

(E and F) Effect of p62 phosphorylation on ImP-induced signaling. HEK293 cells were transfected with GFP p62 wild-type (WT) or GFP p62 T269A/S272A mutant, and incubated with ImP (100 μM) for 2 hr in the absence (E) or presence (F) of amino acids (n = 3). S.E., short exposure, L.E., long exposure.

Data are mean ± SEM. *$p < 0.05$, **$p < 0.01$, ***$p < 0.001$. Unpaired two-tailed Student's t tests.

See also Figure S5.

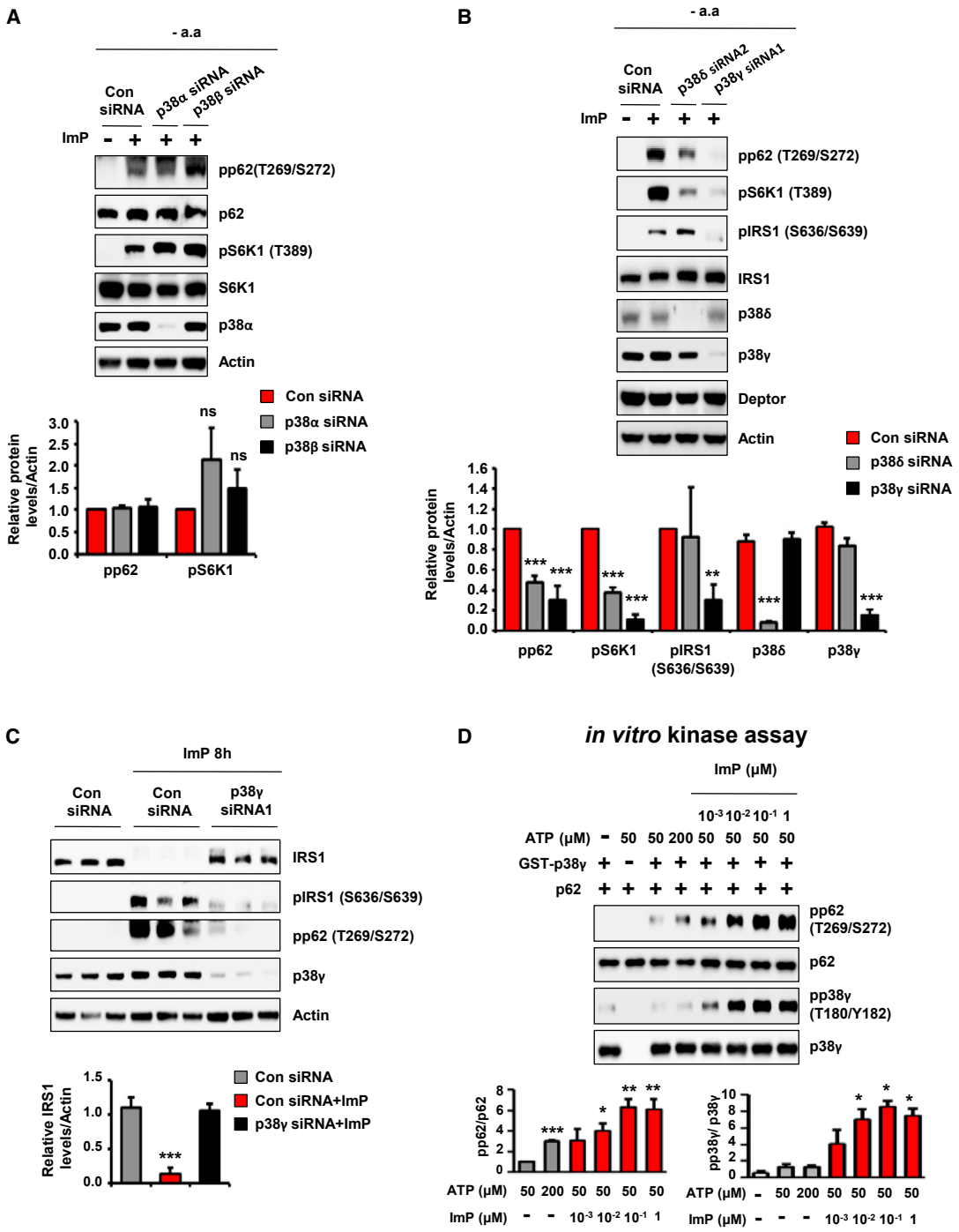

Figure 6. p38γ Is Responsible for Imidazole Propionate Sensing

(A) Effect of conventional p38 knockdown on imidazole propionate (ImP)-induced signaling (n = 3). HEK293 cells were transfected with control siRNA (Con siRNA), p38α siRNA, or p38β siRNA and incubated with ImP (100 μM) in the absence of amino acids (−a.a) for 1 hr.

(B) Effect of alternative p38 knockdown on ImP-induced signaling (n = 3). HEK293 cells were transfected with control siRNA (Con siRNA), p38δ siRNA2, or p38γ siRNA1 and incubated with ImP (100 μM) in the absence of amino acids for 1 hr.

(C) Effect of p38γ depletion on ImP-induced IRS reduction in serum-starved HEK293 cells (n = 6).

(D) *In vitro* kinase assay (n = 3). p38γ and p62 were preincubated and the kinase reaction was started by adding ATP in the absence or presence of ImP.

Data are mean ± SEM. *$p < 0.05$, **$p < 0.01$, ***$p < 0.001$; ns, not significant. One-way ANOVA followed by Dunnett's test (A and B). Unpaired two-tailed Student's t tests (C and D).

See also Figure S6.

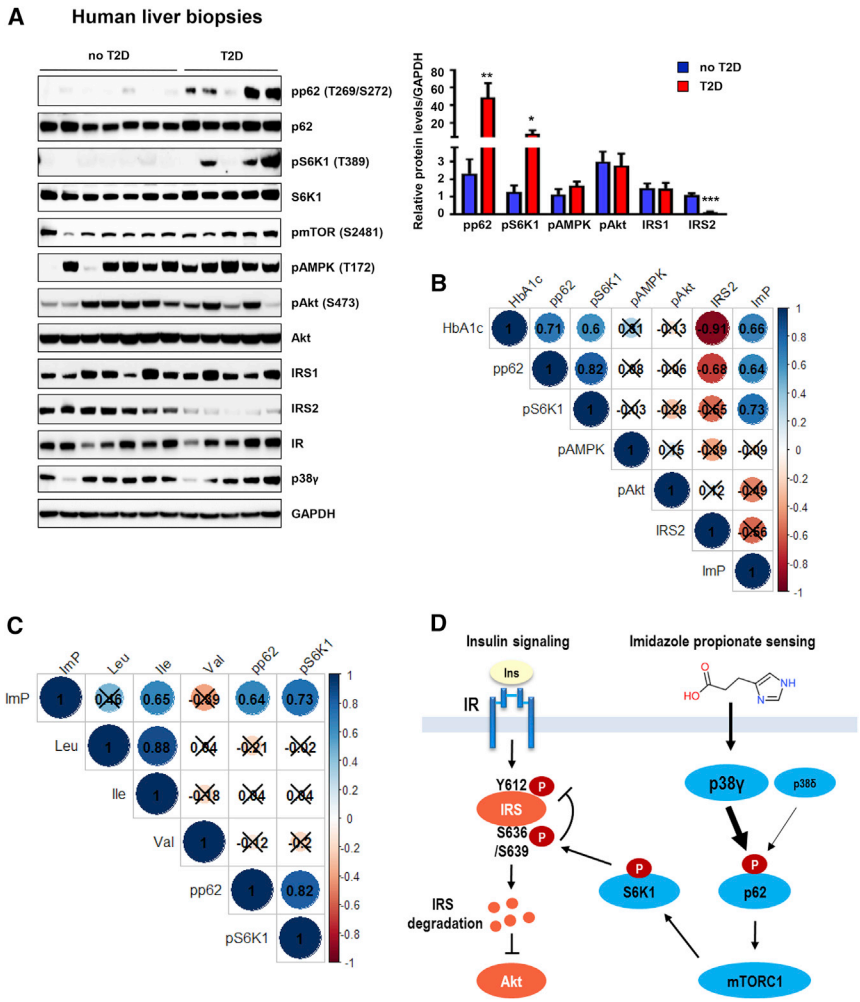

Figure 7. Imidazole Propionate Correlates with p62 and S6K1 Phosphorylation in Human Liver

(A) Immunoblot showing differences in phosphorylation of proteins involved in the mTORC1 pathway in liver biopsies from obese BMI-matched subjects with (T2D, n = 5) or without type 2 diabetes (no T2D, n = 7).

(B) Pearson's correlations between HbA1c, imidazole propionate (ImP), and protein phosphorylation in the human liver (n = 12).

(C) Pearson's correlations between portal levels of ImP or BCAAs (Leu, Ile, or Val) and phosphorylation of p62 or S6K1 in the human liver. Nonsignificant correlations (p value > 0.05) are indicated by crosses.

(D) Schematic depiction of ImP-induced signaling. Data are mean ± SEM. *p < 0.05, **p < 0.01, ***p < 0.001. Unpaired two-tailed Student's t tests (A).

Zhang et al., 2007). It is tempting to speculate that imidazole propionate-induced mTORC1 activation might instead be the link between microbiota, mTORC1 hyperactivation, and human health; future studies that assess the impact on host metabolism of blocking imidazole propionate production in bacteria would test this possibility. Of note, imidazole-based drugs bind to a variety of therapeutic targets (Gaba and Mohan, 2016), suggesting that other signaling pathways can be triggered by imidazole propionate. Thus, further identification of signaling pathways induced by imidazole propionate may reveal drug targets to tackle human disease associated with altered microbial metabolism.

STAR★METHODS

Detailed methods are provided in the online version of this paper and include the following:

- KEY RESOURCES TABLE
- CONTACT FOR REAGENT AND RESOURCE SHARING
- EXPERIMENTAL MODEL AND SUBJECT DETAILS
  - Human study populations
  - Mice
  - Bacterial strains
  - Primary hepatocytes
  - HEK293 cells
- METHOD DETAILS
  - Antibiotic treatment
  - Acute imidazole propionate injection
  - Imidazole propionate pellet implantation
  - TSE system
  - Metabolite analysis
  - *In vitro* gut simulator
  - Batch culture of fecal samples
  - Computational prediction of UrdA-containing bacteria
  - Experimental validation of UrdA-containing bacteria
  - Differential abundance analysis
  - Quantitative real-time PCR analysis
  - Protein analysis
  - Plasmids and siRNAs

- Immunofluorescence
- *In vitro* kinase assay
- Statistical analysis

SUPPLEMENTAL INFORMATION

Supplemental Information includes six figures and five tables and can be found with this article online at https://doi.org/10.1016/j.cell.2018.09.055.

ACKNOWLEDGMENTS

We thank Sung Ho Ryu (Pohang University of Science and Technology, Republic of Korea) and Ying Shiuan Lee for providing materials. We also thank Marie-Louise Ekholm for assistance with the population-based study and Manuela Krämer, Carina Arvidsson, Sara Nordin-Larsson, Ulrica Enquist, and Caroline Wennberg for technical assistance. We are grateful to Anna Hallén for producing the graphical abstract. The computations for metagenomics analyses were performed on resources provided by the Swedish National Infrastructure for Computing (SNIC) through Uppsala Multidisciplinary Center for Advanced Computational Science (UPPMAX). This study was supported by the Novo Nordisk Foundation (NNF15OC0016798) the Swedish Research Council, Swedish Diabetes Foundation, Swedish Heart Lung Foundation, Göran Gustafsson's Foundation, IngaBritt och Arne Lundberg's Foundation, Knut and Alice Wallenberg Foundation, the Swedish Foundation for Strategic Research, the FP7 sponsored program METACARDIS (305312), the regional agreement on medical training and clinical research (ALF) between Region Västra Götaland and Sahlgrenska University Hospital, JPI (A healthy diet for a healthy life; 2017-01996_3), and a grant from a Transatlantic Networks of Excellence Award from the Leducq Foundation (17CVD01) A.K. is supported by a postdoctoral grant from the Wenner-Gren Foundations. M.N. is supported by a ZONMW-VIDI grant 2013 (016.146.327) and CVON Young Talent grant 2012. F.B. is Torsten Söderberg Professor in Medicine and recipient of an ERC Consolidator Grant (European Research Council, Consolidator grant 615362-METABASE).

AUTHOR CONTRIBUTIONS

A.K. and F.B. designed the experiments. A.K., A.M., M.T.K., L.M.-H., A.C., H.J., and L.E.O. performed experiments. M.S. and P.-O.B. measured imidazole propionate levels. H.W. performed the computational analysis. C.S. and G.B. were responsible for inclusion and sampling of the Swedish cohort. V.G., A.H., M.d.B., and M.N. were responsible for inclusion and sampling of the discovery cohort. A.K., R.P., and F.B. wrote the manuscript and all authors approved and commented on the manuscript.

DECLARATION OF INTERESTS

F.B. is founder and shareholder of Metabogen AB. A.K. and F.B. has filed patent based in part on findings in this paper.

Received: March 11, 2018
Revised: June 30, 2018
Accepted: September 26, 2018
Published: October 25, 2018

REFERENCES

Anjani, K., Lhomme, M., Sokolovska, N., Poitou, C., Aron-Wisnewsky, J., Bouillot, J.L., Lesnik, P., Bedossa, P., Kontush, A., Clement, K., et al. (2015). Circulating phospholipid profiling identifies portal contribution to NASH signature in obesity. J. Hepatol. *62*, 905–912.

Aronov, P.A., Luo, F.J.G., Plummer, N.S., Quan, Z., Holmes, S., Hostetter, T.H., and Meyer, T.W. (2011). Colonic contribution to uremic solutes. J. Am. Soc. Nephrol. *22*, 1769–1776.

Ashwell, J.D. (2006). The many paths to p38 mitogen-activated protein kinase activation in the immune system. Nat. Rev. Immunol. *6*, 532–540.

Beardmore, V.A., Hinton, H.J., Eftychi, C., Apostolaki, M., Armaka, M., Darragh, J., McIlrath, J., Carr, J.M., Armit, L.J., Clacher, C., et al. (2005). Generation and characterization of p38beta (MAPK11) gene-targeted mice. Mol. Cell. Biol. *25*, 10454–10464.

Beenstock, J., Ben-Yehuda, S., Melamed, D., Admon, A., Livnah, O., Ahn, N.G., and Engelberg, D. (2014). The p38β mitogen-activated protein kinase possesses an intrinsic autophosphorylation activity, generated by a short region composed of the α-G helix and MAPK insert. J. Biol. Chem. *289*, 23546–23556.

Bender, R.A. (2012). Regulation of the histidine utilization (hut) system in bacteria. Microbiol. Mol. Biol. Rev. *76*, 565–584.

Benjamini, Y., and Hochberg, Y. (1995). Controlling the false discovery rate - a practical and powerful approach to multiple testing. J. R. Stat. Soc. Series B Stat. Methodol. *57*, 289–300.

Blagosklonny, M.V. (2013). TOR-centric view on insulin resistance and diabetic complications: perspective for endocrinologists and gerontologists. Cell Death Dis. *4*, e964.

Bogachev, A.V., Bertsova, Y.V., Bloch, D.A., and Verkhovsky, M.I. (2012). Urocanate reductase: identification of a novel anaerobic respiratory pathway in Shewanella oneidensis MR-1. Mol. Microbiol. *86*, 1452–1463.

Camacho, C., Coulouris, G., Avagyan, V., Ma, N., Papadopoulos, J., Bealer, K., and Madden, T.L. (2009). BLAST+: architecture and applications. BMC Bioinformatics *10*, 421.

Chen, Q., and Reimer, R.A. (2009). Dairy protein and leucine alter GLP-1 release and mRNA of genes involved in intestinal lipid metabolism in vitro. Nutrition *25*, 340–349.

Copp, J., Manning, G., and Hunter, T. (2009). TORC-specific phosphorylation of mammalian target of rapamycin (mTOR): phospho-Ser2481 is a marker for intact mTOR signaling complex 2. Cancer Res. *69*, 1821–1827.

Cotillard, A., Kennedy, S.P., Kong, L.C., Prifti, E., Pons, N., Le Chatelier, E., Almeida, M., Quinquis, B., Levenez, F., Galleron, N., et al.; ANR MicroObes consortium (2013). Dietary intervention impact on gut microbial gene richness. Nature *500*, 585–588.

Cuenda, A., and Rousseau, S. (2007). p38 MAP-kinases pathway regulation, function and role in human diseases. Biochim. Biophys. Acta *1773*, 1358–1375.

Dodd, D., Spitzer, M.H., Van Treuren, W., Merrill, B.D., Hryckowian, A.J., Higginbottom, S.K., Le, A., Cowan, T.M., Nolan, G.P., Fischbach, M.A., and Sonnenburg, J.L. (2017). A gut bacterial pathway metabolizes aromatic amino acids into nine circulating metabolites. Nature *551*, 648–652.

Duran, A., Amanchy, R., Linares, J.F., Joshi, J., Abu-Baker, S., Porollo, A., Hansen, M., Moscat, J., and Diaz-Meco, M.T. (2011). p62 is a key regulator of nutrient sensing in the mTORC1 pathway. Mol. Cell *44*, 134–146.

Esposito, D.L., Li, Y., Cama, A., and Quon, M.J. (2001). Tyr(612) and Tyr(632) in human insulin receptor substrate-1 are important for full activation of insulin-stimulated phosphatidylinositol 3-kinase activity and translocation of GLUT4 in adipose cells. Endocrinology *142*, 2833–2840.

Finn, R.D., Clements, J., and Eddy, S.R. (2011). HMMER web server: interactive sequence similarity searching. Nucleic Acids Res. *39*, W29-37.

Finn, R.D., Coggill, P., Eberhardt, R.Y., Eddy, S.R., Mistry, J., Mitchell, A.L., Potter, S.C., Punta, M., Qureshi, M., Sangrador-Vegas, A., et al. (2016). The Pfam protein families database: towards a more sustainable future. Nucleic Acids Res. *44* (D1), D279–D285.

Gaba, M., and Mohan, C. (2016). Development of drugs based on imidazole and benzimidazole bioactive heterocycles: recent advances and future directions. Med. Chem. Res. *25*, 173–210.

Ge, B., Gram, H., Di Padova, F., Huang, B., New, L., Ulevitch, R.J., Luo, Y., and Han, J. (2002). MAPKK-independent activation of p38alpha mediated by TAB1-dependent autophosphorylation of p38alpha. Science *295*, 1291–1294.

González-Terán, B., Matesanz, N., Nikolic, I., Verdugo, M.A., Sreeramkumar, V., Hernández-Cosido, L., Mora, A., Crainiciuc, G., Sáiz, M.L., Bernardo, E., et al. (2016). p38γ and p38δ reprogram liver metabolism by modulating neutrophil infiltration. EMBO J. *35*, 536–552.

Harrington, L.S., Findlay, G.M., Gray, A., Tolkacheva, T., Wigfield, S., Rebholz, H., Barnett, J., Leslie, N.R., Cheng, S., Shepherd, P.R., et al. (2004). The TSC1-2 tumor suppressor controls insulin-PI3K signaling via regulation of IRS proteins. J. Cell Biol. *166*, 213–223.

Kanehisa, M., and Goto, S. (2000). KEGG: kyoto encyclopedia of genes and genomes. Nucleic Acids Res. *28*, 27–30.

Karlsson, F.H., Tremaroli, V., Nookaew, I., Bergström, G., Behre, C.J., Fagerberg, B., Nielsen, J., and Bäckhed, F. (2013). Gut metagenome in European women with normal, impaired and diabetic glucose control. Nature *498*, 99–103.

Karlsson, F.H., Nookaew, I., and Nielsen, J. (2014). Metagenomic data utilization and analysis (MEDUSA) and construction of a global gut microbial gene catalogue. PLoS Comput. Biol. *10*, e1003706.

Kikuchi, M., Ueno, M., Itoh, Y., Suda, W., and Hattori, M. (2017). Uremic toxin-producing gut microbiota in rats with chronic kidney disease. Nephron *135*, 51–60.

Kim, L., Del Rio, L., Butcher, B.A., Mogensen, T.H., Paludan, S.R., Flavell, R.A., and Denkers, E.Y. (2005). p38 MAPK autophosphorylation drives macrophage IL-12 production during intracellular infection. J. Immunol. *174*, 4178–4184.

Kim, Y.M., Stone, M., Hwang, T.H., Kim, Y.G., Dunlevy, J.R., Griffin, T.J., and Kim, D.H. (2012). SH3BP4 is a negative regulator of amino acid-Rag GTPase-mTORC1 signaling. Mol. Cell *46*, 833–846.

Koeth, R.A., Wang, Z., Levison, B.S., Buffa, J.A., Org, E., Sheehy, B.T., Britt, E.B., Fu, X., Wu, Y., Li, L., et al. (2013). Intestinal microbiota metabolism of L-carnitine, a nutrient in red meat, promotes atherosclerosis. Nat. Med. *19*, 576–585.

Koh, A., De Vadder, F., Kovatcheva-Datchary, P., and Bäckhed, F. (2016). From dietary fiber to host physiology: short-chain fatty acids as key bacterial metabolites. Cell *165*, 1332–1345.

Kumar, S., Stecher, G., and Tamura, K. (2016). MEGA7: molecular evolutionary genetics analysis version 7.0 for bigger datasets. Mol. Biol. Evol. *33*, 1870–1874.

Larkin, M.A., Blackshields, G., Brown, N.P., Chenna, R., McGettigan, P.A., McWilliam, H., Valentin, F., Wallace, I.M., Wilm, A., Lopez, R., et al. (2007). Clustal W and Clustal X version 2.0. Bioinformatics *23*, 2947–2948.

Layman, D.K., and Walker, D.A. (2006). Potential importance of leucine in treatment of obesity and the metabolic syndrome. J. Nutr. *136* (1, Suppl), 319S–323S.

Le Chatelier, E., Nielsen, T., Qin, J., Prifti, E., Hildebrand, F., Falony, G., Almeida, M., Arumugam, M., Batto, J.M., Kennedy, S., et al.; MetaHIT consortium (2013). Richness of human gut microbiome correlates with metabolic markers. Nature *500*, 541–546.

Leontieva, O.V., Demidenko, Z.N., and Blagosklonny, M.V. (2014). Rapamycin reverses insulin resistance (IR) in high-glucose medium without causing IR in normoglycemic medium. Cell Death Dis. *5*, e1214.

Linares, J.F., Duran, A., Reina-Campos, M., Aza-Blanc, P., Campos, A., Moscat, J., and Diaz-Meco, M.T. (2015). Amino acid activation of mTORC1 by a PB1-domain-driven kinase complex cascade. Cell Rep. *12*, 1339–1352.

Liu, R., Hong, J., Xu, X., Feng, Q., Zhang, D., Gu, Y., Shi, J., Zhao, S., Liu, W., Wang, X., et al. (2017). Gut microbiome and serum metabolome alterations in obesity and after weight-loss intervention. Nat. Med. *23*, 859–868.

Love, M.I., Huber, W., and Anders, S. (2014). Moderated estimation of fold change and dispersion for RNA-seq data with DESeq2. Genome Biol. *15*, 550.

Mishima, E., Fukuda, S., Mukawa, C., Yuri, A., Kanemitsu, Y., Matsumoto, Y., Akiyama, Y., Fukuda, N.N., Tsukamoto, H., Asaji, K., et al. (2017). Evaluation of the impact of gut microbiota on uremic solute accumulation by a CE-TOFMS-based metabolomics approach. Kidney Int. *92*, 634–645.

Mojtahedi, M.C., Thorpe, M.P., Karampinos, D.C., Johnson, C.L., Layman, D.K., Georgiadis, J.G., and Evans, E.M. (2011). The effects of a higher protein intake during energy restriction on changes in body composition and physical function in older women. J. Gerontol. A Biol. Sci. Med. Sci. *66*, 1218–1225.

Muto, Y., Sato, S., Watanabe, A., Moriwaki, H., Suzuki, K., Kato, A., Kato, M., Nakamura, T., Higuchi, K., Nishiguchi, S., et al.; Long-Term Survival Study (LOTUS) Group (2006). Overweight and obesity increase the risk for liver cancer in patients with liver cirrhosis and long-term oral supplementation with branched-chain amino acid granules inhibits liver carcinogenesis in heavier patients with liver cirrhosis. Hepatol. Res. *35*, 204–214.

Ozes, O.N., Akca, H., Mayo, L.D., Gustin, J.A., Maehama, T., Dixon, J.E., and Donner, D.B. (2001). A phosphatidylinositol 3-kinase/Akt/mTOR pathway mediates and PTEN antagonizes tumor necrosis factor inhibition of insulin signaling through insulin receptor substrate-1. Proc. Natl. Acad. Sci. USA *98*, 4640–4645.

Pedersen, H.K., Gudmundsdottir, V., Nielsen, H.B., Hyotylainen, T., Nielsen, T., Jensen, B.A., Forslund, K., Hildebrand, F., Prifti, E., Falony, G., et al.; MetaHIT Consortium (2016). Human gut microbes impact host serum metabolome and insulin sensitivity. Nature *535*, 376–381.

Qin, L.Q., Xun, P., Bujnowski, D., Daviglus, M.L., Van Horn, L., Stamler, J., and He, K.; INTERMAP Cooperative Research Group (2011). Higher branched-chain amino acid intake is associated with a lower prevalence of being overweight or obese in middle-aged East Asian and Western adults. J. Nutr. *141*, 249–254.

Qin, J., Li, Y., Cai, Z., Li, S., Zhu, J., Zhang, F., Liang, S., Zhang, W., Guan, Y., Shen, D., et al. (2012). A metagenome-wide association study of gut microbiota in type 2 diabetes. Nature *490*, 55–60.

Ridaura, V.K., Faith, J.J., Rey, F.E., Cheng, J., Duncan, A.E., Kau, A.L., Griffin, N.W., Lombard, V., Henrissat, B., Bain, J.R., et al. (2013). Gut microbiota from twins discordant for obesity modulate metabolism in mice. Science *341*, 1241214.

Rui, L., Fisher, T.L., Thomas, J., and White, M.F. (2001). Regulation of insulin/insulin-like growth factor-1 signaling by proteasome-mediated degradation of insulin receptor substrate-2. J. Biol. Chem. *276*, 40362–40367.

Sancak, Y., Peterson, T.R., Shaul, Y.D., Lindquist, R.A., Thoreen, C.C., Bar-Peled, L., and Sabatini, D.M. (2008). The Rag GTPases bind raptor and mediate amino acid signaling to mTORC1. Science *320*, 1496–1501.

Schröder, I., Gunsalus, R.P., Ackrell, B.A.C., Cochran, B., and Cecchini, G. (1991). Identification of active site residues of Escherichia coli fumarate reductase by site-directed mutagenesis. J. Biol. Chem. *266*, 13572–13579.

Schroeder, B.O., and Bäckhed, F. (2016). Signals from the gut microbiota to distant organs in physiology and disease. Nat. Med. *22*, 1079–1089.

Shah, O.J., and Hunter, T. (2006). Turnover of the active fraction of IRS1 involves raptor-mTOR- and S6K1-dependent serine phosphorylation in cell culture models of tuberous sclerosis. Mol. Cell. Biol. *26*, 6425–6434.

Shoaie, S., Ghaffari, P., Kovatcheva-Datchary, P., Mardinoglu, A., Sen, P., Pujos-Guillot, E., de Wouters, T., Juste, C., Rizkalla, S., Chilloux, J., et al.; MICRO-Obes Consortium (2015). Quantifying diet-induced metabolic changes of the human gut microbiome. Cell Metab. *22*, 320–331.

Smith, M.I., Yatsunenko, T., Manary, M.J., Trehan, I., Mkakosya, R., Cheng, J., Kau, A.L., Rich, S.S., Concannon, P., Mychaleckyj, J.C., et al. (2013). Gut microbiomes of Malawian twin pairs discordant for kwashiorkor. Science *339*, 548–554.

Soliman, G.A., Acosta-Jaquez, H.A., Dunlop, E.A., Ekim, B., Maj, N.E., Tee, A.R., and Fingar, D.C. (2010). mTOR Ser-2481 autophosphorylation monitors mTORC-specific catalytic activity and clarifies rapamycin mechanism of action. J. Biol. Chem. *285*, 7866–7879.

Sonnenburg, J.L., and Bäckhed, F. (2016). Diet-microbiota interactions as moderators of human metabolism. Nature *535*, 56–64.

Suárez-Zamorano, N., Fabbiano, S., Chevalier, C., Stojanović, O., Colin, D.J., Stevanović, A., Veyrat-Durebex, C., Tarallo, V., Rigo, D., Germain, S., et al. (2015). Microbiota depletion promotes browning of white adipose tissue and reduces obesity. Nat. Med. *21*, 1497–1501.

Tzatsos, A. (2009). Raptor binds the SAIN (Shc and IRS-1 NPXY binding) domain of insulin receptor substrate-1 (IRS-1) and regulates the phosphorylation of IRS-1 at Ser-636/639 by mTOR. J. Biol. Chem. *284*, 22525–22534.

van der Heiden, C., Wadman, S.K., de Bree, P.K., and Wauters, E.A. (1972). Increased urinary imidazolepropionic acid, N-acetylhistamine and other imidazole compounds in patients with intestinal disorders. Clin. Chim. Acta *39*, 201–214.

Wallner, S., Winkler, A., Riedl, S., Dully, C., Horvath, S., Gruber, K., and Macheroux, P. (2012). Catalytic and structural role of a conserved active site histidine in berberine bridge enzyme. Biochemistry *51*, 6139–6147.

Wang, X., Beugnet, A., Murakami, M., Yamanaka, S., and Proud, C.G. (2005). Distinct signaling events downstream of mTOR cooperate to mediate the effects of amino acids and insulin on initiation factor 4E-binding proteins. Mol. Cell. Biol. *25*, 2558–2572.

Wang, Z., Klipfell, E., Bennett, B.J., Koeth, R., Levison, B.S., Dugar, B., Feldstein, A.E., Britt, E.B., Fu, X., Chung, Y.M., et al. (2011). Gut flora metabolism of phosphatidylcholine promotes cardiovascular disease. Nature *472*, 57–63.

Windey, K., De Preter, V., and Verbeke, K. (2012). Relevance of protein fermentation to gut health. Mol. Nutr. Food Res. *56*, 184–196.

Wu, H., Esteve, E., Tremaroli, V., Khan, M.T., Caesar, R., Mannerås-Holm, L., Ståhlman, M., Olsson, L.M., Serino, M., Planas-Fèlix, M., et al. (2017). Metformin alters the gut microbiome of individuals with treatment-naive type 2 diabetes, contributing to the therapeutic effects of the drug. Nat. Med. *23*, 850–858.

Yang, Q., and Guan, K.L. (2007). Expanding mTOR signaling. Cell Res. *17*, 666–681.

Zhang, Z.Y., and Dixon, J.E. (1993). Active site labeling of the Yersinia protein tyrosine phosphatase: the determination of the pKa of the active site cysteine and the function of the conserved histidine 402. Biochemistry *32*, 9340–9345.

Zhang, Y., Guo, K., LeBlanc, R.E., Loh, D., Schwartz, G.J., and Yu, Y.H. (2007). Increasing dietary leucine intake reduces diet-induced obesity and improves glucose and cholesterol metabolism in mice via multimechanisms. Diabetes *56*, 1647–1654.

Zhang, W., Sargis, R.M., Volden, P.A., Carmean, C.M., Sun, X.J., and Brady, M.J. (2012). PCB 126 and other dioxin-like PCBs specifically suppress hepatic PEPCK expression via the aryl hydrocarbon receptor. PLoS ONE *7*, e37103.

STAR★METHODS

KEY RESOURCES TABLE

REAGENT or RESOURCE	SOURCE	IDENTIFIER
Antibodies		
Rabbit anti-phospho-Akt (Ser473) (1:1000)	Cell Signaling	Cat# 4058; RRID: AB_331168
Rabbit anti-phospho-Akt (Thr308) (1:500)	Cell Signaling	Cat# 9275; RRID: AB_329828
Rabbit anti-phospho-p70 S6 kinase (Thr389) (1:500)	Cell Signaling	Cat# 9205; RRID: AB_330944
Rabbit p70 S6 kinase (1:500)	Cell Signaling	Cat# 9202; RRID: AB_331676
Rabbit anti-phospho-IRS-1 (Ser636/Ser639) (1:500)	Cell Signaling	Cat# 2388; RRID: AB_330339
Rabbit anti-phospho-SQSTM1/p62 (Thr269/Ser272)	Cell Signaling	Cat# 13121; RRID: AB_2750574
Rabbit anti-phospho-mTOR (Ser2481) (1:500)	Cell Signaling	Cat# 2974S; RRID: AB_2231885
Rabbit anti-phospho-mTOR (Ser2448) (1:500)	Cell Signaling	Cat# 2971; RRID: AB_330970
Rabbit anti-mTOR (1:100)	Cell Signaling	Cat# 2983; RRID: AB_2105622
Rabbit anti-DEPTOR/DEPDC6 (D9F5) (1:500)	Cell Signaling	Cat# 11816; RRID: AB_2750575
Rabbit anti-SQSTM1/p62 (1:500)	Cell Signaling	Cat# 5114; RRID: AB_10624872
Rabbit anti-insulin receptor β (4B8) (1:500)	Cell Signaling	Cat# 3025; RRID: AB_2280448
Rabbit anti-IRS-2 (1:500)	Cell Signaling	Cat# 4502; RRID: AB_2125774
Rabbit anti-IRS-2 (1:500)	Thermo Fisher	Cat# PA5-14897; RRID: AB_2125800
Rabbit anti-p38γ MAPK (1:500)	Cell Signaling	Cat# 2307; RRID: AB_10860779
Rabbit anti-phospho-p38 MAPK (Thr180/Tyr182) (1:500)	Cell Signaling	Cat# 9211; RRID: AB_331641
Rabbit anti-p38α MAPK (1:500)	Cell Signaling	Cat# 9218; RRID: AB_330731
Rabbit anti-Akt (pan) (11E7) (1:500)	Cell Signaling	Cat# 4685; RRID: AB_2225340
Rabbit anti-GAPDH (14C10) (1:500)	Cell Signaling	Cat# 2118; RRID: AB_561053
Rabbit anti-β-Actin (13E5) (1:500)	Cell Signaling	Cat# 4970; RRID: AB_2223172
Rabbit anti-IRS1 (1:500)	EMD Millipore	Cat# 06-248; RRID: AB_2127890
Goat anti-SAPK4 (p38δ) (1:500)	Santa Cruz	Cat# sc-7585; RRID: AB_656012
Mouse anti-c-Myc (9E10) (1:1000)	Santa Cruz	Cat# sc-40; RRID: AB_627268
Mouse anti-HA-probe (F-7) (1:1000)	Santa Cruz	Cat# sc-7392; RRID: AB_627809
Rabbit anti-Flag (1:1000)	Sigma-Aldrich	Cat# F7425; RRID: AB_439687
Mouse anti-LAMP2 (H4B4) (1:100)	Abcam	Cat# ab25631; RRID: AB_470709
Rabbit anti-GFP (1:1000)	Sigma-Aldrich	Cat# SAB4301138; RRID: AB_2750576
Rabbit anti-phospho-IRS1 (Tyr612) (1:500)	EMD Millipore	Cat# 09-432; RRID: AB_1163457
Rabbit anti-phospho-S6 (Ser235/Ser236)	Cell Signaling	Cat# 4858; RRID: AB_916156
Rabbit anti-LC3B (1:500)	Cell Signaling	Cat# 2775; RRID: AB_915950
Rabbit anti-phospho-AMPK (T172) (1:500)	Cell Signaling	Cat# 2535; RRID: AB_331250
HRP-linked anti-rabbit IgG (1:2500)	GE Healthcare	Cat# NA934-1ML; RRID: AB_2750578
HRP-linked anti-mouse IgG (1:2500)	GE Healthcare	Cat# NA9310-1ML; RRID: AB_772193
Bacterial and Virus Strains		
Escherichia coli	N/A	K12
Bifodobacterium longum	NESTLE	NCC2705
Aerococcus urinae	CCUG	59500

(*Continued on next page*)

Continued

REAGENT or RESOURCE	SOURCE	IDENTIFIER
Streptococus mutans	CCUG	69401
Anaerococcus prevotii	CCUG	41932 T
Adlercreutzia equolifaciens	CCUG	54925 T
Eggerthella lenta	CCUG	17323 AT
Lactobacillus paraplantarum	CCUG	35983 T
Brevibacillus laterosporus	CCUG	52899
Shewanella oneidensis MR-1	ATCC	700550
Biological Samples		
Human portal plasma	Clinical Trials	N/A
Human peripheral plasma	Clinical Trials	N/A
Human liver biopsies	Clinical Trials	N/A
Chemicals, Peptides, and Recombinant Proteins		
Imidazole propionate (deamino histidine)	Santa Cruz	sc294276; CAS 1074-59-5
Urocanate (4-imidazoleacrylic acid)	Santa Cruz	sc214246; CAS 104-89-3
Histidine	Santa Cruz	sc394101; CAS 71-00-1
Indole propionate	Santa Cruz	sc255215; CAS 830-96-6
Ampicillin	Sigma-Aldrich	A9518
Metronidazole	Sigma-Aldrich	M3761
Vancomycin	Sigma-Aldrich	V2002
Neomycin	Sigma-Aldrich	N6386
Streptomycin	Sigma-Aldrich	S6501
Bacitracin	Sigma-Aldrich	11702
Ciprofloxacin	Sigma-Aldrich	PHR1167
Ceftazidime	Sigma-Aldrich	A6987
Collagenase type IV	Sigma-Aldrich	C5138
Dulbecco's modified Eagle's medium	Lonza	BE12614F
Ham's F-12 Nutrient Mix	Hyclone	10235122
Fetal bovine serum	Hyclone	SV30160.03
Earle's Balanced Salt Solution	GIBCO	24010-043
Penicillin/Streptomycin	Hyclone	SV30010
RPMI-HEPES 1640	Lonza	BE12115F
Dexamethasone	Sigma-Aldrich	D8893
Poly-L-lysine	Sigma-Aldrich	P6282
Rapamycin	Merk Millipore	553210
Torin1	Cell Signaling	14379S
Lipofectamine 2000	Thermo Fisher	11668019
Solg™ Pfu-X DNA polymerase	SolGent Co	SPX16-R500
Recombinant p62	Abcam	ab95320
Recombinant p38γ	Abcam	ab125651
Tris (Trizma Base)	Sigma-Aldrich	T6066
NaCl	Sigma-Aldrich	S3014
EDTA	Sigma-Aldrich	EDS
Sodium orthovanadate	Sigma-Aldrich	S6508
Sodium fluoride	Sigma-Aldrich	201154
PMSF	Sigma-Aldrich	P7626
glycerophosphate	Sigma-Aldrich	G5422
glycerol	Sigma-Aldrich	G7893

(*Continued on next page*)

Continued

REAGENT or RESOURCE	SOURCE	IDENTIFIER
CHAPS	Thermo Fisher	28300
Complete mini, EDTA free protease inhibitor cocktail	Sigma-Aldrich	11836170001
ATP	Sigma-Aldrich	A2383
MOPS	Sigma-Aldrich	M1254
Beta-glycerol-phosphate	Sigma-Aldrich	50020
DTT	Sigma-Aldrich	D9163
Human insulin, Actrapid Penfill	Novo Nordisk	A10AB01
Glucose	Fresenius Kabi	B05BA03
Custom made slow-releasing pellets	Innovative Research of America	N/A
Acetonitrile	Thermo Fisher	10001334
1-Butanol	Sigma-Aldrich	1.01988
1-Butanol-d_{10}	Sigma-Aldrich	302996
Hydrochloric acid (37%)	Sigma-Aldrich	258148-M
Yeast extract	Oxoid	LP0021
Arabinogalactan	Sigma-Aldrich	10830
Pectin	Sigma-Aldrich	76282
Xylan	TCI	X0078 (CAS # 9014-63-5)
Starch	Sigma-Aldrich	S9765-250
Proteose peptone	Sigma-Aldrich	82450
Mucin	Sigma-Aldrich	M2378
Cysteine	Sigma-Aldrich	W326305
di-potasium hydrogen phosphate	Sigma-Aldrich	P3786
di-hydrogen potasium phosphate	Merck	1.04873.0250
Calcium chloride dihydrate	Merck	1.02382.0500
Magnesium sulfate heptahydrate	Merck	A171286
Hemin	Sigma-Aldrich	51280
Sodium bicarbonate	Merck	1.06329.0500
Bile	Sigma-Aldrich	B3883
Pancreatin	Sigma-Aldrich	P3292
Pepsin	Sigma-Aldrich	P6887
Biotin	Sigma-Aldrich	B4639
Cobalamin	Sigma-Aldrich	V2876
4-Aminobenzoic acid	Sigma-Aldrich	A9878
Folic acid	Sigma-Aldrich	F8758
Pyridoxamine dihydrochloride	Sigma-Aldrich	P9158
Riboflavin	Sigma-Aldrich	R9504
Thiamine-HCl	Sigma-Aldrich	T1270
Glucose/microbiology	Merck	346351
Brain heart infusion	Oxoid	CM1135B
Enhanced chemiluminescence	Thermo Fisher	WBKLS0500
Critical Commercial Assays		
RNeasy Mini Kit	QIAGEN	74106
1X SYBR Green Master Mix	Thermo Fisher	4309155
High Capacity cDNA Reverse Transcription kit	Thermo Fisher	4368814
NuPAGE Novex 4-12% Bis-Tris Gels	Invitrogen	NP0336BOX

(*Continued on next page*)

Continued

REAGENT or RESOURCE	SOURCE	IDENTIFIER
Novex 4-20% Tris-Glycine Mini gels	Invitrogen	XP04205BOX
Ultra-sensitive mouse insulin ELISA	Crystal Chem	90080
Experimental Models: Cell Lines		
HEK293	ATCC	CRL-1573
Primary hepatocytes	Male C57BL/6J	N/A
Experimental Models: Organisms/Strains		
Male C57BL/6J	N/A	N/A
Oligonucleotides		
Table S5	N/A	N/A
Recombinant DNA		
Myc-Rag GTPases	Dr. Do-Hyung Kim	Kim et al., 2012
GFP p62 WT	Dr. Sung Ouk Kim	University of Western Ontario, London, Ontario, Canada
GFP p62 T269A/S272A	In this study	N/A
Flag mTOR	Dr. Sung Ho Ryu	Pohang University of Science and Technology, Republic of Korea
HA raptor	Dr. Sung Ho Ryu	Pohang University of Science and Technology, Republic of Korea
Software and Algorithms		
Prism (version 7)	GraphPad	N/A
R Software	Ross Ihaka and Robert Gentleman https://www.r-project.org/	N/A
MEGA (version 7)	Kumar et al., 2016	N/A
Clustal X	Larkin et al., 2007	N/A
BLASTP	Camacho et al., 2009	N/A
HMM profiling	Finn et al., 2011	N/A
Pfam domain scan	Finn et al., 2016	N/A
DESeq2	Love et al., 2014	N/A
Other		
CFX96 Real-Time PCR Detection	Bio-Rad	C1000
TissueLyser II	QIAGEN	85300
Laser scanning confocal imaging	Carl Zeiss	N/A
Black Stone pump and controller	Hanna Instruments, UK	BL7916-2
pH electrode	Hanna Instruments, UK	HI-2910B/5
Proton exchange membrane	Membrane International, NJ	CMI-7000S
Peristaltic pump	Bio-Rad	EP-1 Econo
Coy chamber	COY Laboratory Products	http://coylab.com/products/anaerobic-chambers/vinyl-anaerobic-chambers/
Micro tube 1.3ml K3E	SARSTEDT	41.1504.105
Microvette CB 300 Z	SARSTEDT	16.440.100
Glucose meters	Bayer Contour XT	ASCENSIA Diabetes Care
TSE systems	Bad Homburg, Germany	PhenoMaster system
UPLC column C18 (2.1x100mm 1.7μ)	Waters	186002352
UPLC pump (Infinity 1290)	Agilent	G4204A
QTRAP 5500	Sciex	N/A
HTC/PAL Autosampler	CTC analytics	N/A
Multitube Vortex	VWR	444-7061

(*Continued on next page*)

Continued

REAGENT or RESOURCE	SOURCE	IDENTIFIER
Centrifuge	Eppendorf	5430R
Nitrogen evaporator	Techne	FSC400D
Nitrocellulose membrane (0.45 μm pore)	Invitrogen	LC2001

CONTACT FOR REAGENT AND RESOURCE SHARING

Further information and requests for resources and reagents should be directed to and will be fulfilled by the Lead Contact, Fredrik Bäckhed (fredrik@wlab.gu.se).

EXPERIMENTAL MODEL AND SUBJECT DETAILS

Human study populations

Two human cohorts were used in this study

The first cohort comprised 5 obese subjects with type 2 diabetes and 10 BMI-matched subjects without type 2 diabetes who were undergoing laparoscopic Roux-and-Y gastric bypass surgery at the Slotervaart Hospital, Amsterdam, the Netherlands (Table S1). All of the subjects with type 2 diabetes were on metformin treatment and two of these were also on insulin treatment. Subjects were fasted overnight before the morning of the surgery, and a peripheral venous sample was taken just before the patient went into the operating room. Anthropometric measurements and a stool sample were also taken before surgery. During the surgery, a portal vein sample (vena puncture) was taken as previously described (Anjani et al., 2015) and liver biopsies were also obtained. Fasting glucose (by glucose meters, Roche Diagnostics), insulin (by an electrochemiluminescence immunoassay, Roche Modular System), and HbA1c (Menarini Diagnostic) were measured in the peripheral blood plasma. All participants gave informed consent before the surgery and the protocol was approved by the Medical Ethical Committee of the Slotervaart Hospital, Amsterdam, the Netherlands.

The second cohort comprised 649 subjects from a randomly selected population sample of adults aged 50 to 64 years and living in the Gothenburg area, Sweden. These subjects were recruited from the census register. Exclusion criteria were: known diabetes; inflammatory diseases, such as Crohn's disease, ulcerative colitis, rheumatic diseases; treatment with steroids or immunomodulatory drugs; cancer (unless relapse free for the preceding 5 years); cognitive dysfunction. A 75 g oral glucose tolerance test (OGTT) was performed in the morning after an overnight fast, and fasting- and 2-h post load capillary blood glucose were measured. Subjects fulfilling criteria for type 2 diabetes were re-examined with a repeated OGTT within 3 weeks. Subjects were included in the study if they were found to have impaired fasting glucose (n = 119), impaired glucose tolerance (n = 142), or type 2 diabetes (n = 53). In addition, approximately every fifth subject with normal glucose tolerance was included (n = 335). Blood samples were obtained from all the participants. Examinations took place at the Wallenberg Laboratory, University of Gothenburg, Sweden. All participants gave informed consent and the study was approved by the Ethics Committee at Gothenburg University.

Both men and women were included in both study cohorts. However, due to the relative few individuals in the first cohort we could not perform separate analyses of men and women. In the second cohort we corrected the results for potential confounders such as sex. In agreement, separate analyses of imidazole propionate levels in men and women revealed that the metabolite was elevated in both men (7.6 ± 0.5 nM versus 15.1 ± 1.2 nM; $p < 0.001$) and women (11.2 ± 0.6 nM versus 24.9 ± 5.8 nM; $p < 0.001$) with type 2 diabetes compared with controls with normal glucose tolerance.

Mice

10-15-week-old male GF and CONVR C57BL/6J mice were used in the animal experiments. GF mice were maintained in flexible film isolators under a strict 12 h light cycle and all mice had unlimited access to water and food. GF status was routinely tested by culturing fecal bacteria anaerobically and aerobically and also was verified regularly by PCR for bacterial 16S rDNA using the primers 27 F and 1492 R (Key Resources Table). PCR reactions were performed with a 5-min preincubation at 95°C followed by 30 cycles of 30 s at 94°C, 45 s at 52°C, and 90 s at 72°C and then kept at 72°C for 7 min. All mice were fed an autoclaved chow diet (5021 LabDiet) *ad libitum*. All mice experiments were performed in our animal facility and were approved by the Ethics Committee on Animal Care and Use in Gothenburg, Sweden.

Bacterial strains

Eight representative UrdA-containing bacterial strains (without conserved "H," Key Resources Table) and control strains *Escherichia coli k12* and *Bifidobacterium longum NCC2705* (with conserved "H," Key Resources Table) were maintained on brain-heart infusion (BHI) medium as described below without histidine or urocanate under strict anaerobic conditions in a Coy chamber (5% hydrogen, 10% carbon dioxide and 85% nitrogen) at 37°C.

Primary hepatocytes

Primary hepatocytes were isolated from male C57BL/6J mice by digesting liver with perfusion of collagenase type IV as described previously (Zhang et al., 2012). After perfusion, 16 × 10^5 cells were plated on collagen-coated 60 mm dishes in Dulbecco's modified Eagle's medium (DMEM)/F12 supplemented with fetal bovine serum (FBS), penicillin/streptomycin, and 100 nM dexamethasone. After 4 h, the medium was changed to DMEM/F12 containing penicillin/streptomycin. For insulin stimulation, primary hepatocytes were cultured in DMEM/F12 with or without 100 μM imidazole propionate for 8 to 20 h and treated with 5 nM insulin for the indicated times. For amino acid deprivation, primary hepatocytes were cultured in DMEM/F12 for 24 h, rinsed once with Earle's Balanced Salt Solution (EBSS) and then incubated in EBSS for 1 h before incubation with 100 μM imidazole propionate for the indicated times.

HEK293 cells

For imidazole propionate stimulation in the absence of amino acids, HEK293 cells (ATCC CRL-1573) grown and maintained in 4.5 g/l glucose DMEM with 10% (v/v) FBS were serum-starved for 18 h and then amino acid-deprived with EBSS for 1 h. Otherwise, HEK293 cells grown in RPMI-HEPES with 10% (v/v) FBS were serum-starved for 18 h. For transfection, HEK293 cells cultured in poly-L-lysine-coated 60 mm dish for 18 h were transfected (with plasmids or siRNA as indicated) for 4 h; after replacing the medium, the cells were cultured for another 24 h and then serum-starved for 18 h. For insulin stimulation, serum-starved HEK293 cells were preincubated with imidazole propionate for 8 h and treated with 5 nM insulin.

METHOD DETAILS

Antibiotic treatment

Antibiotic cocktails in drinking water (containing 100 μg/ml neomycin, 50 μg/ml streptomycin, 100 μg/ml ampicillin, 50 μg/ml vancomycin, 100 μg/ml metronidazole, 1 mg/ml bacitracin, 125 μg/ml ciprofloxacin, and 100 μg/ml ceftazidime) were freshly prepared every two days and were given *ad libitum* for 10 days to C57BL/6J CONVR mice. This protocol was chosen since it was reported not to promote loss of body weight (Suárez-Zamorano et al., 2015).

Acute imidazole propionate injection

To test the effect of imidazole propionate on glucose metabolism, 500 μg imidazole propionate in 200 μl water containing 1% DMSO (18 mM) or vehicle (1% DMSO in water) was injected intraperitoneally into GF C57BL/6J mice twice per day for 3 days. For CONVR mice, 100 μg imidazole propionate in 200 μl vehicle (3.6 mM) was used since CONVR mice are continuously exposed to microbial metabolites and have longer retention time of organic solutes compared with GF mice (Mishima et al., 2017). At day 4, mice were injected again with either vehicle or imidazole propionate and then fasted for 4 h. Intraperitoneal glucose tolerance test (1 g/kg body weight, Fresenius Kabi) was then performed after fasting. Blood glucose levels were measured from tail blood using glucose meters (Bayer Contour XT) at 0, 15, 30, 60, and 120 min after glucose injection. Blood samples for analysis of insulin were taken in serum clot activator tubes (Microvette ® CB 300 Z) before and 15 and 30 min after glucose injection. Serum insulin was measured with Ultra-Sensitive mouse Insulin ELISA kit. Plasma samples to measure the levels of imidazole propionate and urocanate were collected from the portal vein and/or vena cava in EDTA-containing tubes (Micro tube 1.3ml K3E) at the end of experiments. Mice were under isoflurane anesthesia and fresh tissues were taken, snap-frozen in liquid nitrogen and stored at −80°C until protein extraction.

Imidazole propionate pellet implantation

To test the long-term consequence of imidazole propionate treatment, slow-releasing pellets containing either placebo or 4.9 mg imidazole propionate (350 μg/day) were implanted subcutaneously under isoflurane anesthesia in CONVR C57BL/6J mice. Pellets were custom-made (by Innovative Research of America, Sarasota, FL) to release either placebo or imidazole propionate continuously for 14 days. Briefly, a small (5 mm) incision was made at the nape of the neck, the pellet was inserted and the incision closed with sutures. After 14 days, an intraperitoneal glucose tolerance test was performed after 4 h fasting as described above. Tissues were snap frozen in liquid nitrogen and stored at −80°C until protein extraction. Plasma samples were collected as described above.

TSE system

To assess the metabolic impact of imidazole propionate on CONVR C57BL/6J mice, food intake, oxygen consumption and locomotor activity were measured using the PhenoMaster system according to the manufacture's recommendation. Mice were single-housed for two days before being transferred to the PhenoMaster cages, and allowed an additional two days to acclimatize to the new cage before taking measurements. Parameters were automatically measured every 15 min for five days. During the measurements, the mice had free access to water and food. Mice were randomly divided into two weight-matched groups and injected intraperitoneally either with imidazole propionate (100 μg) or vehicle twice a day (8 AM and 5 PM) for three days. Measurements of oxygen consumption (VO_2), carbon dioxide production (VCO_2), and energy expenditure ([3.941(VO_2) + 1.106(VCO_2)]/1000) were adjusted to lean body mass, which was determined by MRI (EchoMRI, Houston, TX).

Metabolite analysis

Global metabolite profiling analysis on (1) plasma from portal blood obtained from obese humans with and without type 2 diabetes and (2) plasma from the portal vein and vena cava of C57BL/6J GF and CONVR mice was performed by Metabolon (Durham, NC) using ultra high performance liquid chromatography coupled to tandem mass spectrometry (UPLC-MS/MS). In brief, samples were prepared using the automated MicroLab STAR® system (Hamilton Company). A recovery standard was added before the first step in the extraction process for quality control. Proteins were precipitated with methanol under vigorous shaking for 2 min (Glen Mills GenoGrinder 2000) followed by centrifugation. The resulting extract was divided into five fractions: one for analysis by UPLC-MS/MS with positive ion mode electrospray ionization, one for analysis by UPLC-MS/MS with negative ion mode electrospray ionization, one for LC polar platform, one for analysis by GC-MS, and one sample was reserved for backup. Samples were placed briefly on a TurboVap® (Zymark) to remove the organic solvent. For LC, the samples were stored overnight under nitrogen before preparation for analysis. For GC, each sample was dried under vacuum overnight before preparation for analysis.

For targeted measurement of imidazole propionate and urocanate, plasma samples were extracted with 3 volumes of ice-cold acetonitrile in 1.5 ml polypropylene tube. After vortexing and centrifugation, the supernatant was dried under a gentle flow of nitrogen. The samples were then reconstituted with 5% HCl (37%) in 1-butanol at 70°C for 1 h and dried under a nitrogen flow, allowing n-butyl ester to be formed. After derivatization, the samples were evaporated and reconstituted in 100 μl of water/acetonitrile (90:10) containing 50 nM of internal standards (labeled imidazole propionate and urocanate made from derivatization using d_{10}-labeled butanol). Samples (5 μl) were injected onto a C18 BEH column (2.1x100 mm with 1.7 μm particles; Waters, Milford, MA) and separated using a gradient consisting of water with 0.1% formic acid (A-phase) and acetonitrile with 0.1% formic acid (B-phase). Mass spectrometric analysis was performed using an Infinity 1290 quaternary UPLC pump (Agilent, Santa Clara, CA) coupled to a QTRAP 5500 (Sciex, Concord, Canada). The imidazole propionate and urocanate were detected by multiple reaction monitoring using the transitions 197/81 and 195/93, respectively. For the internal standards, the transitions 206/81 and 204/93 were used. Calibration curves of imidazole propionate and urocanate were made in water and treated the same way as the samples.

To measure imidazole propionate in liver, snap-frozen liver samples (50 mg) were extracted with 500 μL of ice-cold acetonitrile containing internal standards (imidazole propionate-$^{13}C_3$ and urocanate-$^{13}C_3$, Astra Zeneca, Cambridge, UK) in 1.8 ml polypropylene tube containing ceramic beads. After centrifugation, the supernatant was transferred to a Phree SPE 96-well plate (Phenomenex, Torrance, CA) and eluted onto a collection plate via the positive pressure manifold (Biotage AB, Uppsala, Sweden). After drying the eluate, the samples were reconstituted as described above. After derivatization, the samples were evaporated and reconstituted in 500 μl of water/acetonitrile. Samples (5 μl) were then injected and separated as described above. Mass spectrometric analysis was performed using an Acquity UPLC I-class pump (Waters, Milford, MA) coupled to a Xevo TQ-XS (Waters, Milford, MA). The imidazole propionate and urocanate were detected by multiple reaction monitoring using the transitions 197/81 and 195/93, respectively. For the internal standards, the transitions 200/82 and 198/95 were used. Calibration curves of imidazole propionate and urocanate were made in methanol and treated the same way as the samples.

In vitro gut simulator

A simulated human intestinal redox model (SHIRM) was used to directly investigate whether imidazole propionate could be a microbially produced metabolite. SHIRM is a two-chamber fermenter with an anaerobic luminal chamber and an oxygen feeder, which are separated by a CMI-7000S membrane (Membrane International, NJ) and continuously purged with nitrogen and oxygen, respectively. The oxygen chamber contained 100 mM potassium phosphate buffer. The feed for the luminal chamber consisted of (in g/l) arabinogalactan (1.0), pectin (2.0), xylan (1), starch (3.0), glucose (0.4), yeast extract (3.0), peptone (3.0), mucin type II (1.0), NaCl (0.9), KH_2PO_4 (0.45), K_2HPO_4 (0.45), $CaCl_2.2H_2O$ (0.45), $MgSO_4.7H_2O$ (0.09), hemin (0.01) and cysteine (0.5). A vitamin mix [consisting of (in μg/l) biotin (10), cobalamin (10), p-aminobenzoic acid (30), folic acid (50), pyridoxamine (150), riboflavin (50) and thiamine-HCl (50)] was added. To simulate digestion processes, the feed was acidified to a pH of around 2 with 6 M HCl followed by addition of pepsin (10 mg/l) and neutralized with simulated pancreatic juice [(in g/l) $NaHCO_3$ (12.5), Ox gall bile salts (6.0) and pancreatin (0.9)] to pH 6.9. The luminal chamber was continuously fed with SHIRM feed (70:30 mix of the feed and pancreatic juice described above) at a rate giving a retention time of around 24 h and pH was maintained at 6.6-6.9 using a pH controller and dosing pump (Black Stone BL7916-2, Hanna Instruments, UK).

The SHIRM system was inoculated with aliquots of the feces from subjects with and without type 2 diabetes (from the first cohort); feces from each subject were tested in separate experiments. A pre-culture was prepared anaerobically in a Coy chamber (5% hydrogen, 10% carbon dioxide and 85% nitrogen) by adding 2% fecal material to 5 ml of BHI medium containing (in g/l) yeast extract (5), cellobiose (1), maltose (1), cysteine (0.5) and hemin (0.01). The pre-culture was incubated for 3 h at 37°C, and 2% of the pre-culture was seeded into the luminal compartment of the SHIRM. The luminal communities were stabilized for 1 week before histidine challenge. Samples were collected for up to 7 h and imidazole propionate levels were measured as described above.

Batch culture of fecal samples

Fecal samples (100 mg) from donors with and without type 2 diabetes (from both cohorts) were inoculated in 5 ml BHI medium (as described above) and incubated overnight under strict anaerobic conditions in a Coy chamber at 37°C. For the first cohort, we used samples from all five subjects with type 2 diabetes and five subjects without type 2 diabetes selected because they had the lowest concentrations of imidazole propionate and to match for BMI. For the second cohort, we used samples from the three subjects with

treatment-naive type 2 diabetes with the highest imidazole propionate concentrations and three subjects with normal glucose tolerance with imidazole propionate levels lower than the median value in this group (7.1 nM); the subjects selected were also sex- and BMI-matched. After incubation, 1% (v/v) of the respective BHI precultures was inoculated in SHIRM feed (described above) supplemented with 10 mM histidine. After 36 h of incubation, supernatants were used for imidazole propionate and urocanate quantification. To adjust for variations in bacterial growth, urocanate levels were measured and levels of produced imidazole propionate were divided by urocanate levels. Fold-change (36 h/0 h) was calculated using these adjusted values.

Computational prediction of UrdA-containing bacteria

UrdA was previously predicted to encode fumarate reductase because of its high sequence homology to the FAD- and FMN-binding domains of fumarate reductase, succinate dehydrogenase and L-aspartate oxidase (Bogachev et al., 2012). However, structural modeling of the FAD-binding domain from UrdA identified differences in amino acid sequences from those in fumarate reductase, which potentially gives substrate selectivity to urocanate (Bogachev et al., 2012). To screen for potential imidazole propionate-producing bacteria, we focused on amino acid sequences that are conserved in fumarate reductase from *Shewanella oneidensis* but replaced in potential UrdA. Since conserved "H"s in the active sites of enzymes are important for catalysis in various enzymes (Schröder et al., 1991; Wallner et al., 2012; Zhang and Dixon, 1993), we focused on tyrosine 373 (Y373) in the FAD active sites of UrdA [Y373 corresponds to histidine (H) in fumarate reductase]. Extensive protein screening followed by accurate domain alignment (Figure S2A) identified the existence of 812 UrdA homologs in 670 bacterial genomes (Table S4). Of those, 639 were identified to have an "H" residue in their active sites whereas 173 have non-"H" residues such as "Y" or "M" (Table S4 and Figure S2B).

As shown in Figure S2A, 27 seed protein sequences [including 22 from KEGG annotations (Kanehisa and Goto, 2000)] with high identity to UrdA from *S. oneidensis MR-1* were used to screen potential UrdA homologs among 16,403,888 proteins extracted from 4893 bacterial genomes. These data were downloaded from the NCBI ftp site ftp://ftp.ncbi.nlm.nih.gov/genomes/all/ on June 26, 2016. 658 protein hits were identified using BLASTP program (Camacho et al., 2009) (with the following settings: E value = 1e-4; identity = 30%; coverage = 70%) and those hits were further used as seeds to perform both the second round of protein BLAST and HMM profiling (Finn et al., 2011) (with at least 50% coverage and score larger than 200), resulting in 2230 and 2526 protein hits, respectively. A further Pfam domain scan (Finn et al., 2016) on all identified UrdA candidates revealed that 1774 sequences possess FAD domains. We thus extracted the FAD active sites of UrdA from *S. oneidensis MR-1* (extended to 30 amino acids upstream and downstream of Y373) and performed a third round of protein BLAST against the 1774 FAD-containing hits using the extracted Y373-containing domain as the query sequence. 812 protein hits were identified as the final UrdA homologs. Additional domain alignment was performed using ClustalX (Larkin et al., 2007) to annotate the corresponding active sites (Table S4 and Figure S2B).

Experimental validation of UrdA-containing bacteria

Eight representative UrdA-containing bacterial strains (without conserved "H") were further subjected to experimental validation in pure cultures together with *Escherichia coli k12* and *Bifidobacterium longum NCC2705* as control (with conserved "H"). The maximum likelihood tree was based on extracted FAD domains from all 10 bacteria using MEGA (version 7) (Kumar et al., 2016) with default settings.

To assess the imidazole propionate-producing potential of pure bacterial cultures, all strains were maintained on BHI medium (as described above) without histidine or urocanate under strict anaerobic conditions in a Coy chamber (5% hydrogen, 10% carbon dioxide and 85% nitrogen) at 37°C. To test their potential to produce imidazole propionate, a single colony of each bacterial strain was inoculated in BHI medium and, after overnight incubation, 1% of the preculture was inoculated in BHI medium supplemented with 10 mM histidine or urocanate and incubated for 24 h. After incubation, the cell-free supernatant was used for quantification of imidazole propionate.

Differential abundance analysis

The metagenomics analysis was based on the MEDUSA pipeline (Karlsson et al., 2014) for mapping and DESeq2 (Love et al., 2014) for differential abundance analysis as described previously (Wu et al., 2017). 140 out of 143 "non-H" ImP-producing bacterial strains (173 at the gene level) (Table S4) with high-quality draft/complete genomes were extracted from NCBI to construct the genome catalog required for the MEDUSA pipeline. All metagenome sequences were retrieved from a previous study (33 subjects with treatment-naive type 2 diabetes and 43 with normal glucose tolerance; Karlsson et al., 2013) with Sequence Read Archive (sra) accession code ERP002469.

Quantitative real-time PCR analysis

Mouse liver was homogenized in RLT buffer with β-mercaptoethanol using TissueLyser. RNA was isolated using the RNeasy Minikit and reverse transcribed to synthesize cDNA using High Capacity cDNA Reverse Transcription Kit according to the manufacturer's protocol. Real-time PCR was performed using 1X SYBR Green Master Mix using the primers in Key Resources Table.

Protein analysis

Snap-frozen tissues and harvested cells were lysed in buffer A containing 50 mM Tris-HCl (pH 7.4), 150 mM NaCl, 1 mM EDTA, 1 mM Na_3VO_4, 20 mM NaF, 10 mM glycerophosphate, 1 mM PMSF, 10% glycerol, 1% Triton X-100 and protease inhibitor cocktail. For

western blotting, the cell lysates were sonicated and centrifuged at 20,000*g* for 15 min at 4°C, and the supernatant was mixed with 5X Laemmli buffer [0.156 M Tris-HCl (pH 6.8), 25% glycerol, 12.5% β-mercaptoethanol, 12.5% SDS, 0.1% bromophenol blue], followed by heating at 95°C for 10 min. For immunoprecipitation, the cell lysates were obtained in 0.3% CHAPS-containing lysis buffer, sonicated and centrifuged at 20,000*g* for 15 min at 4°C, and the supernatant was incubated with 20 μl of anti-FLAG beads or 2 μg of the anti-HA antibody at 4°C for 4 h or overnight, respectively, under gentle agitation. Immunocomplexes with anti-HA antibody were collected using protein A-Sepharose beads and were eluted with 2X Laemmli buffer with 100 mM DTT, followed by heating at 95°C for 10 min. Samples treated with Laemmli buffer (20-30 μg for cell lysates or 40-50 μg for tissue lysates to detect basal signal) were separated on Bis-Tris gels or Tris-glycine gels (to detect mTOR), transferred to nitrocellulose membrane, and probed with antibodies indicated. The blots were then reacted with HRP-linked anti-rabbit IgG or anti-mouse IgG, followed by enhanced chemiluminescence.

Plasmids and siRNAs

Myc-Rag GTPases constructs were gifts from Dr. Do-Hyung Kim (University of Minnesota, MN) (Kim et al., 2012). The GFP-p62 WT construct was kindly provided by Dr. Sung Ouk Kim (University of Western Ontario, London, Ontario, Canada) and the GFP-p62 T269A/S272A mutant was generated by site-directed mutagenesis using a Solg™ Pfu-X DNA polymerase using the primers p62 T269A/S272A F and R (Key Resources Table). Transfection with plasmids or siRNAs in HEK293 cells was performed using Lipofectamine 2000 according to the manufacturer's instructions.

Immunofluorescence

Cells were grown on poly-L-lysine coated 4 well chamber slides, fixed with 4% paraformaldehyde for 15 min at 37°C, then washed with glycine-PBS and permeablized with 0.3% Triton X-100 for 10 min. After blocking with 3% BSA in PBS, cells were stained for mTOR and LAMP2. Images were obtained by confocal microscope (63X).

In vitro kinase assay

400 ng of recombinant p62 and 200 ng of recombinant p38γ were incubated in a kinase assay buffer [25 mM MOPS (pH 7.2), 12.5 mM beta-glycerol-phosphate, 25 mM $MgCl_2$, 5 mM EGTA, 2 mM EDTA and 1 mM DTT] for 15 min on ice. In a separate tube, 1 mM ATP diluted in a kinase assay buffer was incubated with DMSO or imidazole propionate (final concentration of ATP in the kinase reaction was 50 or 200 μM). The kinase reaction was started by adding ATP with DMSO or imidazole propionate to the p38γ and p62 mixture for 10 min at 30°C, and stopped by adding 5X Laemmli buffer.

Statistical analysis

Wilcoxon rank-sum test was used to test if metabolites in portal blood plasma differed in abundance between subjects with and without type 2 diabetes in the first cohort (untargeted metabolomics); the raw *P values* were adjusted by the Benjamini-Hochberg method (Benjamini and Hochberg, 1995) with a FDR of 0.1. Kruskal-Wallis rank-sum test followed by Dunnett's multiple comparisons was used for targeted comparisons of imidazole propionate among groups with different levels of glucose tolerance in the second cohort. Multiple regression and analysis of variance with corrections for confounding factors BMI, age and sex were used for this larger cohort. Analysis of datasets containing multiple measurements from mice and humans (comparing metabolites in portal and cava blood plasma) was performed with a two-way ANOVA with repeated-measurements. Wilcoxon one-tailed test was done to see if type 2 diabetes-associated microbiota produces higher imidazole propionate from histidine. One-way ANOVA with Tukey's test was performed when comparing three or more groups. Analysis of effects of imidazole propionate on concentrations of different metabolites or mice physiology (energy expenditure or locomotor activity) depending on light/dark cycle was done with a two-way ANOVA with Sidak's multiple comparisons test. Otherwise, unpaired two-tailed Student's t tests were used, as indicated.

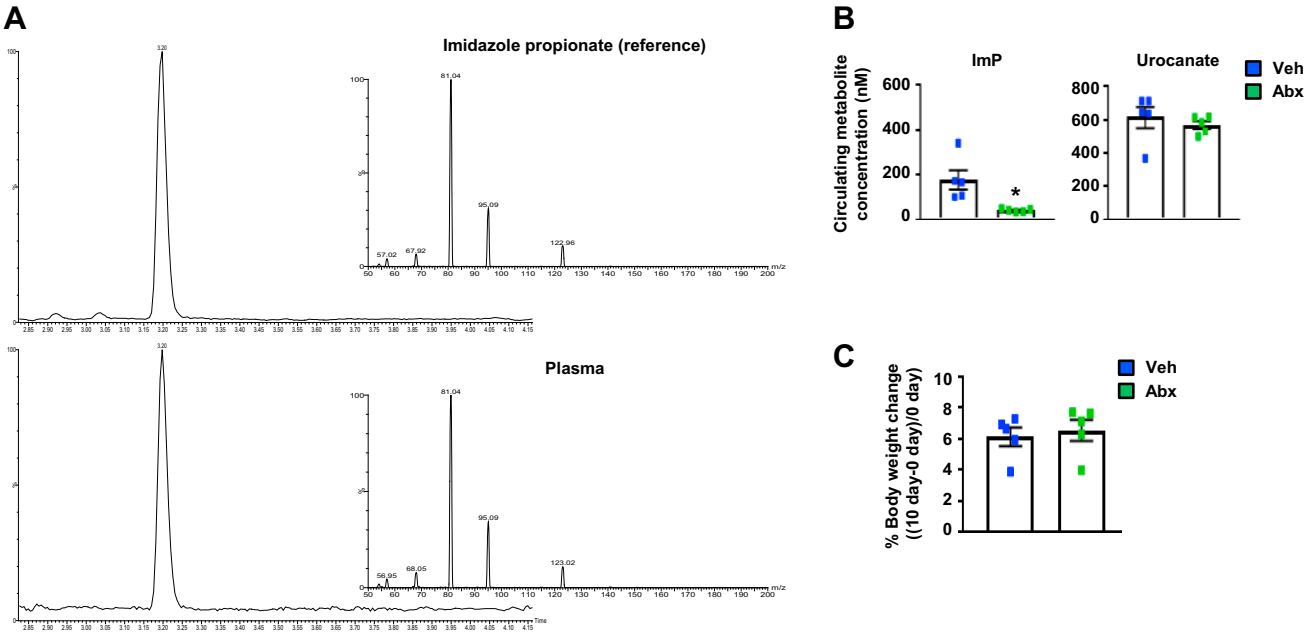

Figure S1. Verification of Imidazole Propionate with Reference Substance and as a Microbiota-Dependent Metabolite, Related to Figure 1

(A) Extracted ion chromatogram and fragmentation pattern of the imidazole propionate reference substance (CAS 1074-59-5, Santa Cruz; upper panel) and imidazole propionate (ImP) in a plasma sample from mice (lower panel).

(B) Peripheral plasma levels of ImP or urocanate in CONVR mice administered with vehicle (Veh, drinking water, n = 5) or an antibiotic cocktail (Abx, n = 5) for 10 days. (C), Percent body weight change 10 days after Abx administration (n = 5 in each group).

Data are mean ± s.e.m. *$p < 0.05$. Unpaired two-tailed Student's t tests (B,C).

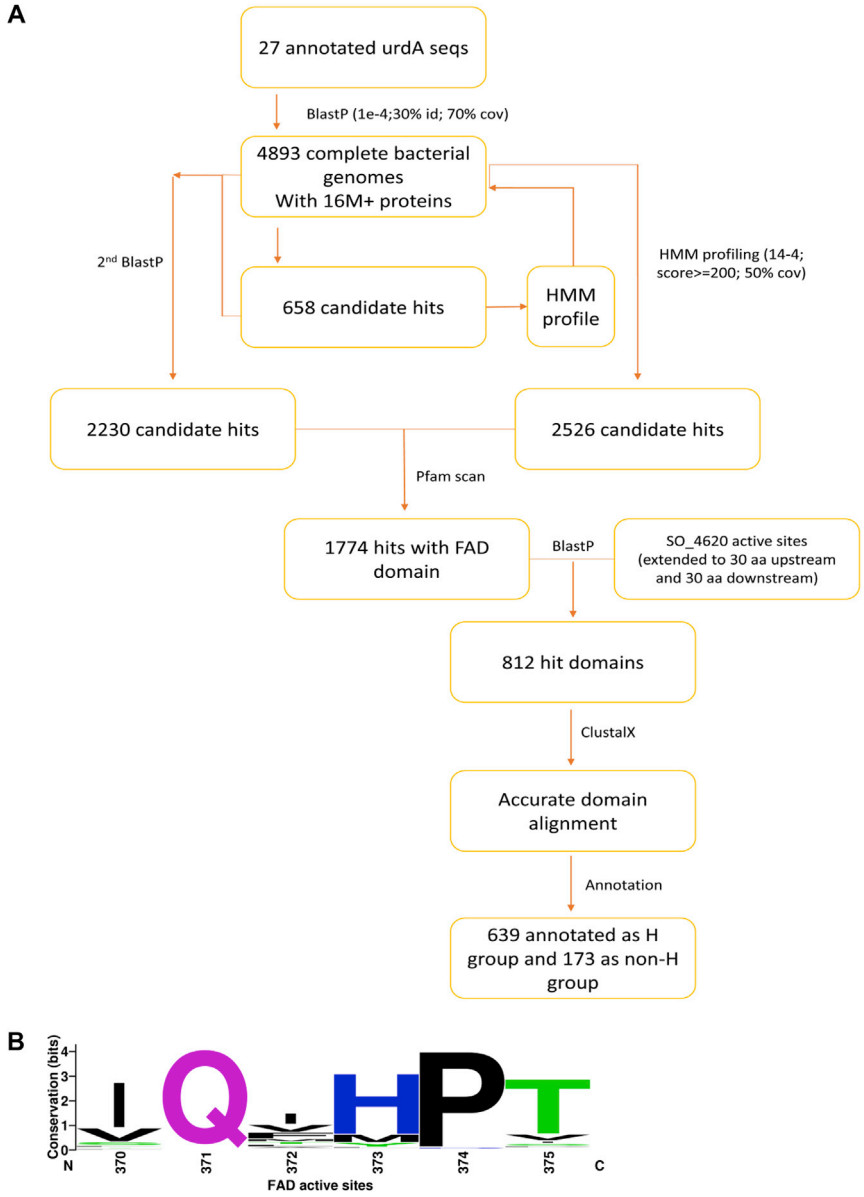

Figure S2. Prediction of Potential UrdA Homologs in Bacterial Genome, Related to Figure 2

(A) Computational prediction of UrdA-containing bacteria.

(B) FAD active sites from potential UrdA homologs.

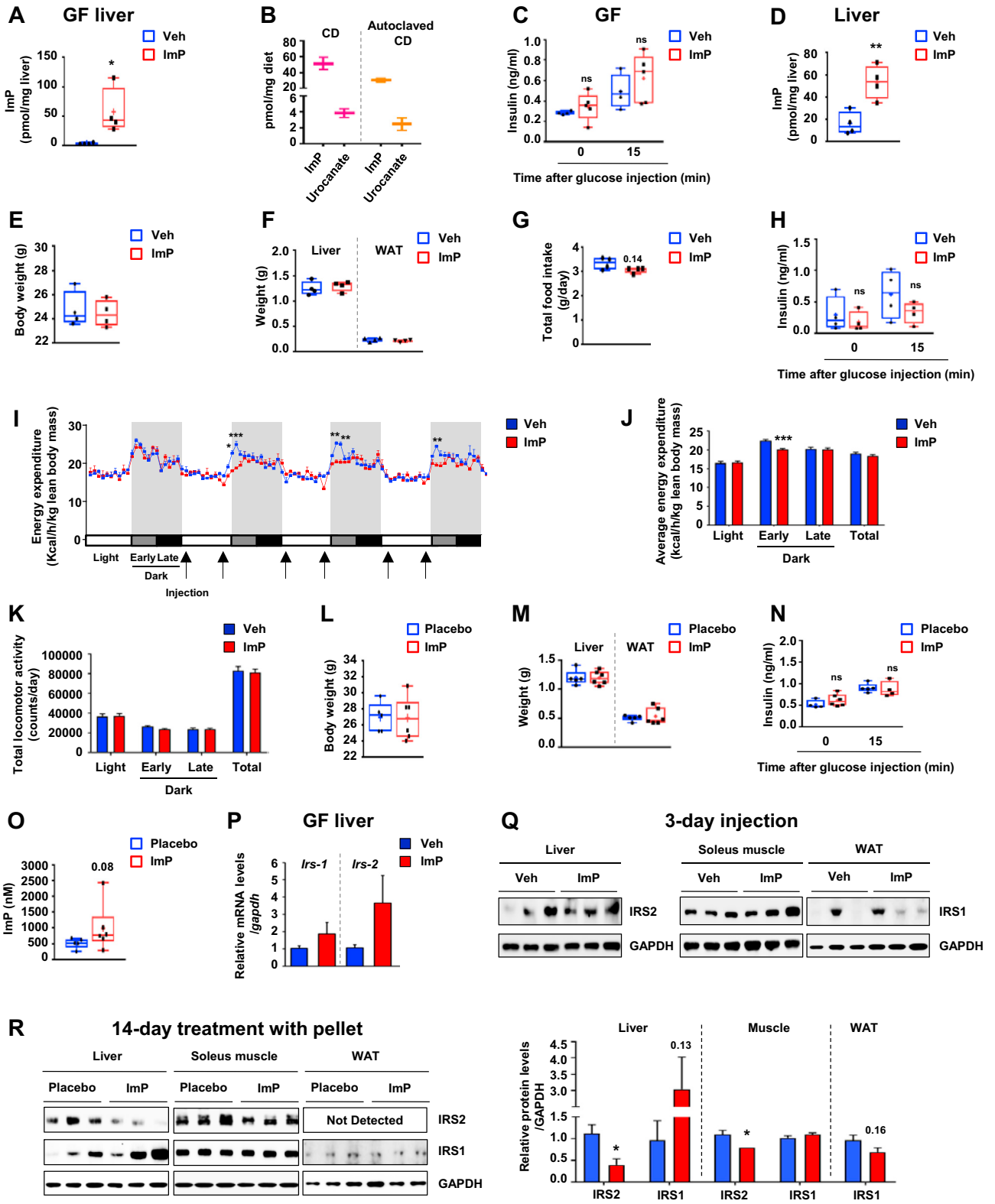

Figure S3. Effects of Imidazole Propionate in Mice, Related to Figure 3

(A) Levels of imidazole propionate (ImP) in the liver of GF mice after intraperitoneal injection of vehicle (Veh, 1% DMSO in water; n = 4) or ImP (500 μg; n = 4) twice per day for 3 days.

(legend continued on next page)

(B) Levels of ImP and urocanate in chow diet (CD) and autoclaved CD.
(C) Serum insulin levels during intraperitoneal glucose tolerance test in GF mice injected with vehicle or ImP for 3 days.
(D) Levels of ImP in the liver of CONVR mice after intraperitoneal injection of vehicle (n = 4) or ImP (100 μg; n = 4) twice per day for 3 days.
(E–H) Effects of ImP on (E), body weight, (F), organ weights (liver and WAT), (G), food intake, and (H), insulin levels after 3-day treatment with vehicle or ImP (100 μg twice per day) in CONVR mice (n = 4).
(I–K) Energy expenditure (I), average energy expenditure (J), and total locomotor activity (K) of CONVR mice injected with vehicle or ImP (100 μg twice per day) for 3 days (n = 4).
(L–O) Effects of long-term ImP on (L), body weight, (M), liver and WAT weights, (N), insulin levels, and (O), circulating levels of ImP 14 days after implanting placebo or ImP pellets.
(P) mRNA levels of *Irs-1* and *Irs-2* in the liver of GF mice after intraperitoneal injection of vehicle (n = 4) or ImP (500 μg; n = 5) twice per day for 3 days.
(Q) Immunoblot of liver, soleus muscle, and WAT lysates from CONVR mice showing effect of 3-day treatment with vehicle or ImP (100 μg twice per day) on IRS (n = 3).
(R) Immunoblot of liver, soleus muscle, and WAT lysates from CONVR mice showing effect of 14-day treatment with placebo or ImP (350 μg per day) on IRS (n = 3).
Data in A-H, L-O are presented as boxplots and show minimum, 25% quartile, median, 75% quartile, and maximum. Data in (J),(K),(P),(R) are mean ± s.e.m. *$p < 0.05$, **$p < 0.01$, ***$p < 0.001$; ns, not significant. Unpaired two-tailed Student's t tests (A-H, L-P, R). Two-way ANOVA followed by Sidak's multiple comparisons test (I). Two-way ANOVA with repeated-measurements followed by Sidak's multiple comparisons test (J,K).

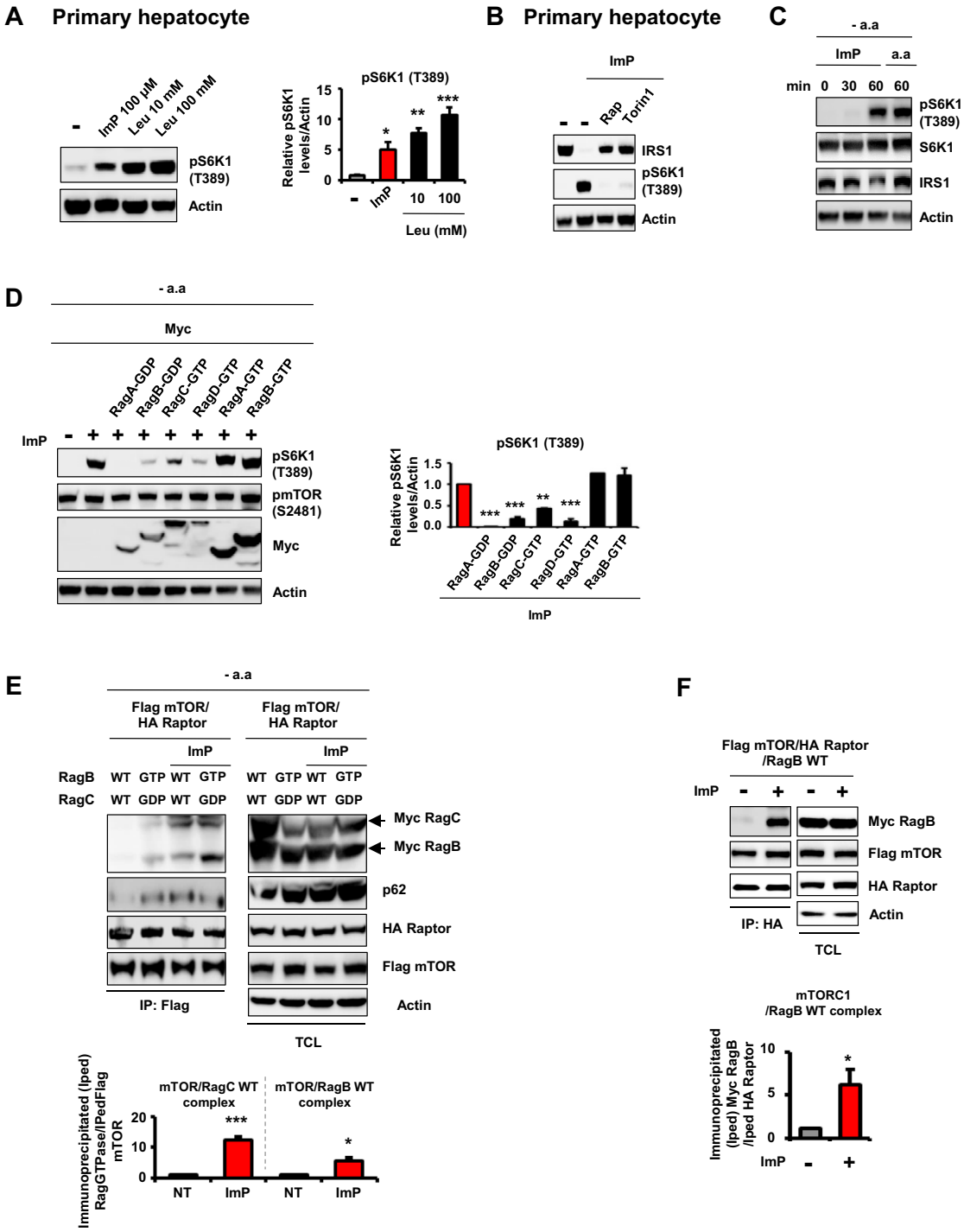

Figure S4. Effects of Imidazole Propionate on mTORC1, Related to Figure 4

(A) Imidazole propionate (ImP) as well as leucine induced mTORC1 activation. Serum-deprived primary hepatocytes were incubated with 10 mM or 100 mM leucine or 100 μM ImP (n = 3).

(B) Rapamycin (Rap, 20 nM) or Torin1 (50 nM) inhibits the effect of ImP (100 μM for 15 h) on IRS and pS6K1 in primary hepatocytes (n = 2).

(C) Rapid effects of ImP (100 μM) on pS6K1 in amino acid-deprived HEK293 cells (n = 2). Serum and amino acid-deprived HEK293 cells were incubated with ImP or amino acids (a.a).

(D) Involvement of Rag GTPases in ImP-induced mTORC1 activation. HEK293 cells were transfected with Myc-tagged constructs as indicated and incubated with 100 μM ImP in the absence of amino acids for 1 h.

(legend continued on next page)

(E) ImP induced Rag GTPases/mTORC1 complex formation. HEK293 cells were co-transfected with FLAG mTOR, HA Raptor, and Myc Rag GTPases and incubated with ImP (100 μM) in the absence of amino acids (-a.a) for 1 h (n = 3). IP: immunoprecipitate, TCL total cell lysate.

(F) ImP induced RagB/mTORC1 complex formation in the presence of amino acids. HEK293 cells expressing Flag mTOR, HA raptor, Myc RagB WT, and GFP p62 were serum starved for 18 h and stimulated with ImP for 2 h (n = 3).

Data are mean ± s.e.m. *$p < 0.05$, **$p < 0.01$, ***$p < 0.001$. Unpaired two-tailed Student's t tests (A, D-F).

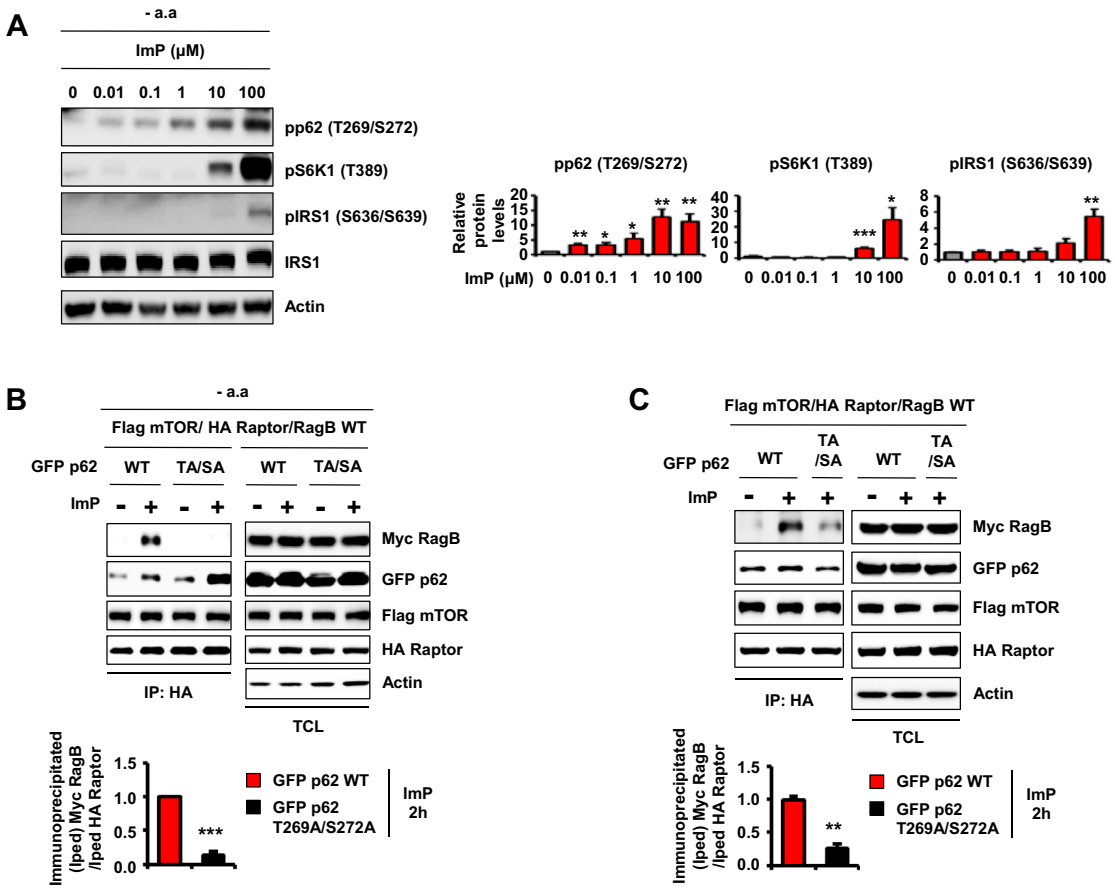

Figure S5. Role of p62 Phosphorylation in ImP-Mediated Signaling, Related to Figure 5

(A) Effect of 1 h treatment with imidazole propionate (ImP) (at the indicated concentrations) on p62, S6K1, and IRS1 phosphorylation in amino acid-deprived HEK293 cells (n = 3-5).

(B and C) Effect of p62 phosphorylation at T269/S272 on ImP-induced mTORC1/RagB complex formation in (B) the absence or (C) the presence of amino acids (n = 3). HEK293 cells expressing Flag mTOR, HA Raptor, Myc RagB WT, and GFP p62 WT or T269A/S272A mutant (TA/SA) were stimulated with ImP for 2 h and then subjected to immunoprecipitation with anti-HA antibody.

Data are mean ± s.e.m. *p < 0.05, **p < 0.01, ***p < 0.001. Unpaired two-tailed Student's t tests (A-C).

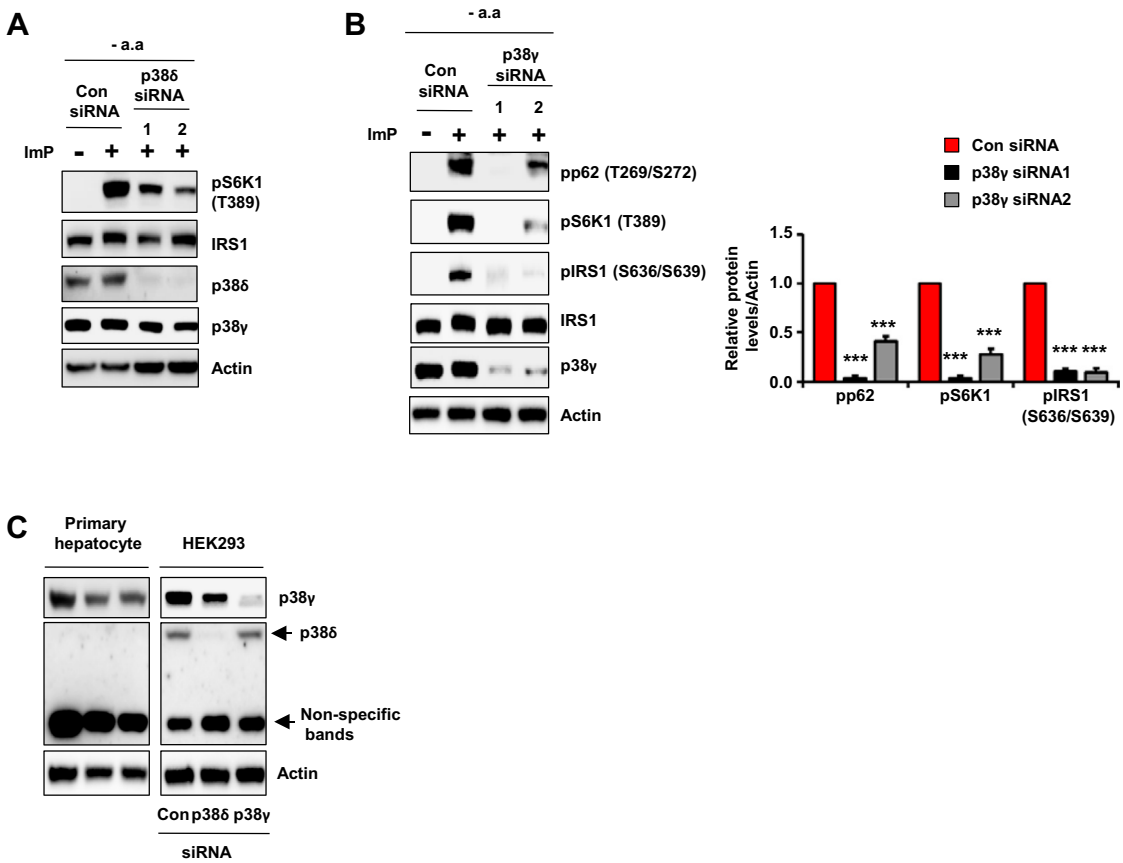

Figure S6. Role of p38γ in ImP-Mediated Signaling, Related to Figure 6

(A) Effects of two distinct non-overlapping siRNAs against p38δ on imidazole propionate (ImP)-induced mTORC1 activation (n = 2).

(B) Effects of two distinct non-overlapping siRNAs against p38γ on ImP-induced signaling (n = 3). HEK293 cells were transfected with control siRNA (Con siRNA) or p38γ siRNA and incubated with ImP (100 μM) in the absence of amino acids for 1.5 h.

(C) Expression of alternative p38 MAPK in primary hepatocytes and HEK293 cells.

Data are mean ± s.e.m. ***$p < 0.001$. One-way ANOVA followed by Dunnett's test (B).